

# STAR CLUSTER DEMOGRAPHICS. I. A GENERAL FRAMEWORK AND APPLICATION TO THE ANTENNAE GALAXIES<sup>1</sup>

BRADLEY C. WHITMORE<sup>2</sup>, RUPALI CHANDAR<sup>3,4</sup>, AND S. MICHAEL FALL<sup>2</sup>

*email: whitmore@stsci.edu, rchandar@ociw.edu, fall@stsci.edu*

## ABSTRACT

We present a framework for understanding the demographics of star cluster systems, and develop a toy model which incorporates a universal initial power law mass function, selected formation histories, selected disruption laws, and a convolution with common artifacts and selection effects found in observational data. A wide variety of observations can be explained by this simple model, including the observed correlation between the brightest young cluster in a galaxy and the total number of young clusters. The model confirms that this can be understood as a statistical size-of-sample effect rather than a difference in the physical process responsible for the formation of the clusters, suggesting that active mergers have the brightest clusters simply because they have the most clusters. A comparison is made between different cluster disruption laws and it is shown that the break in the  $dN/d\tau$  diagram used to determine the parameters in the Boutloukos & Lamers model may be produced by incompleteness near the breakpoint. A model of the Antennae galaxies is developed and compared with the observational data; this extends the mass-age range for cluster comparison over previous studies. An important component of our model is the use of a “two-stage” disruption process, with a very high “infant mortality” rate for the clusters with ages less than  $\approx 10^8$  yrs (i.e., roughly 80%–90% are lost each factor of ten in time,  $\tau$ , independent of mass), and two-body relaxation, which becomes

---

<sup>1</sup>Based on observations with the NASA/ESA *Hubble Space Telescope*, obtained at the Space Telescope Science Institute, which is operated by the Association of Universities for Research in Astronomy, Inc. under NASA contract NAS5-26555.

<sup>2</sup>Space Telescope Science Institute, 3700 San Martin Drive, Baltimore, Maryland 21218

<sup>3</sup>Center for Astrophysical Sciences, Johns Hopkins University, 3400 N. Charles Street, Baltimore, MD 21218

<sup>4</sup>Carnegie Observatories, 813 Santa Barbara St., Pasadena, CA 91101-1292

the dominant disruption mechanism at older ages, preferentially removing the lower mass clusters. Hence, in our model, stars from the dissolved clusters form the field population. We note that a 90 % infant mortality rate for each factor of ten in  $\tau$  (i.e.,  $dN/d\tau \propto \tau^{-1}$ ) is consistent with all measured young cluster populations, including those in the Antennae, Small Magellanic Cloud, and the Milky Way. In fact, the population of clusters in the Antennae can be viewed as a scaled-up version of the Milky Way in many respects, with a scale factor of roughly 1000 times the Lada & Lada sample of embedded star clusters in the local Milky Way. We find no evidence for a truncation of the Antennae cluster mass function at the high mass end.

*Subject headings:* galaxies: star clusters, galaxies: interactions, galaxies: individual (NGC 4038/4039)

## 1. Introduction

The discovery of young massive clusters (hereafter YMCs) in merging and starburst galaxies has been a major catalyst for the field of extragalactic star clusters in recent years (see Whitmore 2003 and Larsen 2005 for reviews). In particular, the fact that the most massive of these young clusters have all the attributes expected of young globular clusters means that we can study the formation of globular clusters in the local universe rather than trying to understand how they formed some 13 Gyr in the past.

A natural inference one might draw from the discovery of YMCs in merging and starburst galaxies is that some “special physics” is occurring in these environments; that normal quiescent spirals can only form low mass open clusters. However, the discovery of a small number of YMCs in normal spiral galaxies by Larsen and Richtler (1999) showed that this inference is incorrect. The formation mechanism required to make YMCs appears to be more “universal” than originally thought. Early hints that this phenomenon might be quite widespread were the discovery of YMCs in barred galaxies (Barth, Ho & Filippenko 1995), M33 (e.g., Chandar, Bianchi, & Ford 1999a,b), and the central region of our own Milky Way Galaxy (Figer et al. 1999). The fact that most studies of the luminosity functions of young compact clusters have found them to be power laws of the form  $\phi(L)dL \propto L^\alpha dL$  with a value of  $\alpha \approx -2$  (e.g., compilations in Whitmore 2003, Larsen 2005, 2006; although see §4.2 for alternative views) provides additional evidence for the universality hypothesis. The main difference appears to be the normalization of the power law, since young active mergers typically have thousands of YMCs, older mergers and starbursts have hundreds of YMCs, and normal spiral galaxies have between zero and one hundred YMCs.

While cluster mass functions have been determined for only a small subset of these galaxies (due to the need for cluster age estimates which are observationally expensive), a similar power law form has been found for the mass and luminosity functions in the Antennae, (i.e.,  $\psi(M)dM \propto M^\beta dM$  with a value of  $\beta \approx -2$ ; Zhang & Fall 1999; Fall 2004; Fall, Chandar, & Whitmore 2006), in the Small and Large Magellanic Clouds (Hunter et al. 2003), as well as a few other galaxies (see review by Larsen 2006).

Since the number of galaxies with sufficient data to form even a meaningful luminosity function was small, Whitmore (2003; originally presented in 2000 as astro-ph/0012546) enlarged his sample by comparing the luminosity of the brightest young cluster in a galaxy with the number of clusters in the system brighter than  $M_V = -9$ . Figure 1 shows an updated version of this figure, with the primary improvements being the addition of galaxies from Tables 1–5 of Larsen (2005) and updated cluster numbers for several galaxies. Although the galaxy sample is heterogeneous, this diagram shows no evidence for a discontinuity in the ability of quiescent spiral galaxies to form bright star clusters, when compared with mergers and starbursts. The observed slope is consistent with the hypothesis that all of the galaxies have the same universal cluster luminosity function; a power law with index  $\approx -2$ . This suggests that active mergers have the brightest clusters only because they have the most clusters (i.e., a size-of-sample effect). *It appears to be a matter of simple statistics rather than a difference in physical formation mechanisms.* A more detailed discussion of Figure 1 is included in §3.1.

While the luminosity and mass functions of young star clusters appear to be power laws, the luminosity and mass functions of old globular clusters are peaked, and are generally characterized with a mean value of  $M_V \approx -7.4$  (corresponding to a mean mass  $\approx 2 \times 10^5 M_\odot$ ) and width  $\sigma \approx 1.4$  mag (e.g., see compilation in Ashman & Zepf 1998). Several theoretical works (Fall & Rees 1977; Vesperini 1998; Fall & Zhang 2001) have studied the effects of two-body relaxation, tidal shocks, and stellar mass loss on cluster populations. These studies have suggested that a natural way to explain this apparent evolution is via the preferential destruction of the fainter, less massive clusters, due primarily to the effects of two-body relaxation in a tidal field. Modelling of this effect has shown preferential dissolution of lower mass clusters hundreds of Myr after they form. Over  $\sim 10$  Gyr this can introduce a turnover in an initial power law mass distribution (e.g., Fall & Zhang 2001), similar to what is observed for ancient globular cluster systems in a number of massive galaxies.

More recently, several studies (e.g., Fall 2004; Whitmore 2004; Fall, Chandar & Whitmore 2005; Bastian et al. 2005; Mengel et al. 2005) have suggested that the majority of stellar clusters are disrupted within the first  $\sim 10$  Myr of life, and hence are presumably not bound to begin with. More specifically, Fall et al. (2005) find that  $dN/d\tau \propto \tau^{-1}$  for clusters

with ages  $\lesssim 100$  Myr and masses  $\gtrsim 3 \times 10^4 M_\odot$  in the Antennae galaxies, implying that roughly 90 % of the clusters are disrupted each decade (i.e., factor of ten) of time,  $\tau$ . This rapid destruction, or “infant mortality”, is the dominant contributor to cluster demographics over this period of time. A similar effect has been noted for  $10^2 - 10^3 M_\odot$  embedded clusters in the Milky Way (Lada & Lada 2003). In apparent contradiction to these results for the young cluster systems in the Antennae and Milky Way, Rafelski & Zaritsky (2005) suggest  $dN/d\tau \propto \tau^{-2}$  for the cluster population in the Small Magellanic Cloud. However, a re-analysis of their data (Chandar et al. 2006) indicates that  $dN/d\tau \propto \tau^{-1}$  in the SMC as well (see §4.3 and Figure 15).

As outlined above, previous results on the Antennae cluster system have provided some of the motivation for the framework presented in the current paper. These have revealed that the mass distribution is approximately independent of age (Zhang & Fall 1999, Fig. 3) and that the age distribution is approximately independent of mass for massive young clusters (Fall et al. 2005, Fig. 2). As in these previous works, we define clusters as the compact, barely-resolved objects detected in galaxies such as the Antennae (e.g., Whitmore et al. 1999). Since we cannot directly assess whether a given aggregate of stars is bound or unbound based on the photometric data alone, we make no assumption about how long a cluster might survive. The development of the model presented here allows us to extrapolate outside of the ranges used previously to establish the cluster mass, age, and luminosity relations, and simultaneously to compare model predictions with the observed properties of the host galaxy. To the degree that our models fit the integrated properties of a galaxy (e.g., the total stellar mass and total luminosity) we can have some confidence that these extrapolations are reasonable.

In summary, it appears plausible that most star clusters form from a universal initial cluster mass function, which is then modified by several disruption mechanisms. The current paper describes a simple toy model designed to test this framework in detail. In order to facilitate direct comparison with observations, common selection effects and data reduction artifacts are included in the model. The results are then compared with observations of the Antennae cluster system which extend the mass-age domain explored previously. An earlier version of some of this work was described in Whitmore (2004). Paper 2 (Chandar & Whitmore 2006, *in preparation*) in this series will extend the comparison to a number of other nearby galaxies, and introduce an objective, 3-dimensional classification system that helps facilitate the comparison (see Whitmore 2004). We are therefore testing a specific view, that most star formation occurs in groups and clusters of stars according to a single power law mass function. This distribution is subsequently modified, with disrupted clusters forming the field. An alternative view is that clusters form with a Gaussian mass function (e.g., Mengel et al. 2005; Gieles et al. 2006; Fritze-van Alvensleben 2004). We discuss the

evidence for and against this possibility in §4.2.

This paper is organized as follows: §2 develops the framework for understanding the observed properties of star cluster populations; §3 presents some results and predictions of the model, in particular a simulation of the  $M_V(\text{brightest})$  vs.  $\log(N)$  diagram, and a comparison with observations of the Antennae galaxies; and §4 discusses broader implications and some potential anomalies for the universal framework. Finally, in §5 we summarize the main conclusions of this work.

## 2. A Universal Framework for Understanding Star Cluster Demographics

In this section we develop a framework for understanding the demographics of star clusters, following the theme outlined in the Introduction. A simple toy model has been created using the IDL programming language to implement this framework. The key ingredients of the model are:

### A. Initial Mass Function

- assumed to be a powerlaw ( $\psi(M)dM \propto M^\beta dM$ ) with index  $\beta = -2$ . The effects of using other indexes are briefly examined in §3.1 and §3.2.

### B. Various Cluster Formation Histories

Two cluster formation histories are included; a constant rate of formation and a Gaussian burst. Different components can be combined together as needed to produce the model for a galaxy. For example, the 5-component model for the Antennae cluster system discussed in §3.2 consists of three constant-formation components and two Gaussian components. All star formation is assumed to occur in clusters. The field stars result from the disruption of the clusters. The Bruzual & Charlot (2003) models are used for the spectral energy distributions [SEDs].

- constant formation in time ( $dN/d\tau = \text{constant}$ )
- Gaussian burst ( $dN/d\tau \propto \tau_0 e^{-\Delta\tau^2/2\sigma^2}$ )

### C. Various Disruption Laws

Four disruption laws are included. It is assumed that the stars from the disrupted clusters become the field stars in the galaxy.

- constant mass loss ( $M = M_0 - \mu_{ev}\tau$ ). This is the time dependence resulting from two-body relaxation for a cluster in the tidal field of the host galaxy (i.e., a value of  $\mu_{ev} \sim 2 \times 10^{-5} M_\odot \text{ yr}^{-1}$  matches the detailed calculations in Fall & Zhang 2001; see their Figures 1 & 4, and their equation 6). We also note that observations of faint globular clusters in the Milky Way (see Fall & Zhang 2001, Figure 3), and M87 (Waters et al. 2006) agree with this functional form.
- constant number loss ( $dN/d\tau \propto \tau^\gamma$ ). A value of  $\gamma = -1$  results in 90 % loss each decade of  $\tau$ ; this is defined as 90% “infant mortality”.
- a two-stage disruption model, incorporating constant number loss (infant mortality) for the first  $10^8$  years and constant mass loss (two-body relaxation) at all ages.
- an empirical disruption law from Boutloukos & Lamers (2003)  
 $(t_{dis}(M_{cl}) = t_4^{dis}(M_{cl}/10^4 M_\odot)^{\gamma_{BL}})$ , where  $t_4^{dis}$  is the disruption time for a  $10^4 M_\odot$  cluster and  $\gamma_{BL}$  is the mass dependence of the disruption timescale.

## D. Convolution with Common Observational Artifacts and Selection Effects

Three artifacts and selection effects are currently incorporated in the model. §2.5 describes the following in more detail, and outlines plans for the inclusion of additional selection effects in the future.

- magnitude threshold
- reddening and extinction
- artifacts from age-dating algorithms

As briefly mentioned in the Introduction, the mass and age distributions for massive young clusters in the Antennae, which provided some of the motivation for this work, are *independent* of one another (Fall 2006). This means that the joint distribution  $g(M, \tau)$  must be the product of the mass and age distributions,  $\psi(M)$  and  $\chi(\tau)$ , which roughly follow the relation  $g(M, \tau) \propto M^\beta \tau^\gamma$ . We have adopted this approach, hence simplifying our model.

We should note that these relationships are only meant to be first-order approximations to reality, designed to develop a simple framework that captures the dominant mechanisms required to understand the demographics of star clusters in galaxies. For example, Fall, Chandar & Whitmore (2006) show that a value of  $\beta \sim -2$  is a reasonable overall fit to the

data for the young ( $\lesssim 100$  Myr) Antennae cluster system over the mass range  $10^4 M_\odot$  to  $10^6 M_\odot$ . The framework presented here allows us to test whether a value of  $\beta \sim -2$  beyond this range is consistent with other available data and our assumed model.

## 2.1. Initial Mass Function

The choice of a power law with index  $\beta = -2$  for the initial distribution of mass has already been motivated in the Introduction. We address recent claims that the initial cluster mass function in some nearby galaxies deviates significantly from a power law in §4.2. One nice attribute of adopting  $\beta = -2$  is that the number of clusters in each decade of decreasing mass increases by a factor of 10, hence there is equal mass in each decade (e.g., the total mass of all the clusters in the range  $10^5 - 10^6 M_\odot$  is the same as the total mass of all the clusters in the range  $10^3 - 10^4 M_\odot$ ).

A word about boundary conditions is in order, since integrating a power law mass function with an index of  $-2$  over all mass ranges would lead to an infinite mass. The lower mass limit is controlled by the masses of individual stars, roughly  $0.1 - 100 M_\odot$ . The highest mass cluster formed may be controlled by statistics, namely the very low probability of producing a cluster with more than  $10^7 M_\odot$ , or possibly by physics if there is a physical upper limit to the allowed mass for an individual cluster. Therefore, there are  $\approx 5 - 8$  decades (i.e., factors of ten) of cluster masses to be concerned with. Hence, if the majority of stars are born in star clusters, each decade in initial mass of the clusters should produce roughly 10–20 % of the total mass in stars for a given galaxy.

One may argue that the mass of stars in globular clusters in the Milky Way is only about  $10^{-4}$  of the total mass of the Galaxy halo, rather than the  $\approx 40-60$  % expected from the argument above and the fact that globular clusters span roughly three decades in mass (from  $\approx 10^4$  to  $\approx 10^7 M_\odot$ ). However, as we shall see, this is consistent with the dominating role that cluster disruption plays in determining the demographics of clusters. Hence, most of the stars initially formed in clusters eventually end up in the field.

We also note that our observations in galaxies like the Antennae only allow us to determine directly the initial mass function over about two decades of mass, from  $\approx 10^4$  to  $10^6 M_\odot$ . However, to the degree that our models fit the integrated properties of a galaxy (e.g., the total stellar mass and total luminosity) we can have some confidence that extrapolations outside of these ranges are reasonable.

## 2.2. Cluster Formation Histories

Our model accomodates linear combinations of constant cluster formation and Gaussian bursts to reproduce observations of different galaxies. For example, typical spiral galaxies can be modeled by an initial burst of star formation to produce the ancient GC population roughly 13 Gyr ago, combined with a constant rate of formation since that time.

We begin our examination of the cluster formation history with perhaps the simplest model; constant formation over the past 13 Gyr with no cluster disruption. Figure 2a (upper panel) shows the  $\log(M/M_\odot)$  vs.  $\log\tau$  diagram for this model, using our standard initial mass function which has a power law with index  $\beta = -2.0$ .

We note that, similar to our choice of  $-2$  for the power law index for the mass distribution, the choice of a constant formation rate simplifies the accounting, since there are a factor of 10 more clusters in each decade of time, by definition. Similarly, the boundary conditions in the temporal dimension are fixed, since clusters (and the brightest stars within them) require  $\approx 1$  Myr to form. Hence, there are only about 4 decades in  $\tau$  to integrate over (i.e.,  $\sim 1$  Myr to  $\sim 10$  Gyr).

Observations of cluster systems are limited by the quality of the data. While cluster detection is a complicated function of object brightness, local background level and complexity, and object size, the most basic observable parameter which sets the limit for a given dataset is the brightness of an object (i.e., the magnitude threshold). Figure 2b (middle panel) shows the same simulation as Figure 2a, but with a magnitude threshold imposed by restricting the simulated sample to clusters with  $M_V \leq -9$ . A comparison of Figures 2a and 2b demonstrates the importance of the magnitude threshold. For example, if this selection effect is not considered, one might conclude that the disruption of faint clusters is the reason for the lack of objects in the bottom right of Figure 2b. This is a cautionary reminder that we must be careful not to confuse evidence for disruption with artifacts caused by observational selection effects. We will return to this point in §2.3.

Figures 2a and 2b also provide a good opportunity for demonstrating the size-of-sample effect. Taken at face value, this figure suggests that massive clusters were only produced in the distant past, since the most massive cluster with an age less than 10 Myr is  $\approx 10^4 M_\odot$ . However, the clusters *were all taken from the same power law mass function*; the only reason for the lack of massive young clusters is the factor of 1000 fewer clusters in the 1 – 10 Myr bin when compared with the 1 – 10 Gyr bin. Hence statistics, rather than physics, are responsible for the lack of massive young clusters in Figure 2. There are simply not enough young clusters to produce the  $2\sigma$  statistical deviation required to form a  $10^5 M_\odot$  cluster, let alone the  $3\sigma$  deviation required for a  $10^6 M_\odot$  cluster.



Figure 2c (bottom panel) shows the same model as Figure 2b, but plotting the luminosity (rather than the mass) versus age. This diagram is more directly related to observations, and serves as a reminder that the magnitude threshold (defined by the lower edge seen horizontally in Figure 2c) translates to a diagonal line in Figure 2b due to the dimming of the clusters with age.

### 2.3. Inclusion of Various Cluster Disruption Laws

At present, four idealized disruption laws have been incorporated into the toy model, as outlined in §2. In Figure 3, we plot age versus mass distributions for simulated clusters for three of the laws (the fourth, the two-stage disruption model, is a combination of two of the other laws, and will be discussed in more detail in §3.2). Each model shown in Figure 3 begins with a constant rate of cluster formation, which is subsequently modified by the various disruption laws described below. Figure 4 shows the corresponding age distributions for the twelve models presented in Figure 3.

In the constant *mass* loss models (shown in the left columns of Figures 3 and 4), a fixed amount of mass is removed from each cluster during each unit of time. A value of  $\mu_{ev} \sim 10^{-5} M_{\odot}/\text{yr}$  results in reasonable values (e.g., a  $10^4 M_{\odot}$  cluster is disrupted in  $10^9$  years). The resulting mass distribution of surviving clusters after a Hubble time looks similar to a typical distribution of globular clusters, with a turnover around  $10^5 M_{\odot}$ , as shown in Figure 5. The constant mass loss disruption law was motivated by the detailed calculations made in Fall & Zhang (2001), which shows that two-body relaxation is the dominant destruction mechanism for clusters older than about  $10^8$  yrs, and that the mass loss of a cluster via two-body relaxation is linear with age. The peak in the mass distribution will also increase linearly with time, as shown in the  $10^{-5} M_{\odot}/\text{yr}$  panel of Figure 3 (which mirrors the result in Fall & Zhang 2001 Figures 3–11). We note that two-body relaxation alone destroys very few clusters in the first  $10^8$  yrs (cf. Baumgardt & Makino 2003), which is contrary to the important role “infant mortality” plays in the evolution of cluster systems.

Models of constant *number* loss, or “infant mortality”, reduce the existing population of clusters by a fixed percentage (for e.g., 0%, 50%, 80%, or 90% *each decade* in  $\tau$ ; corresponding to slopes of  $\gamma = 0.0, -0.3, -0.7$ , and  $-1.0$  for the age distribution). This type of (mass-independent) cluster disruption model is motivated by the age distribution of clusters observed originally in the Antennae (as described in detail in Fall et al. 2005, and further discussed in §2.4). The center column of panels in Figures 3 and 4 show illustrative examples for different values of constant number loss. Over the first  $\sim 10$  Myr in the life of a cluster, photoionization, stellar winds, and supernovae can inject sufficient energy into the

inter-cluster medium to remove much of the gas. This gas removal can unbind the cluster (e.g., Hills 1980; Lada, Margulis & Dearborn 1984; Boily & Kroupa 2003a,b; Fall et al. 2005). Following this stage, stellar evolution will continue to significantly remove mass from the cluster for longer periods of time (e.g., Applegate 1986; Chernoff & Weinberg 1990; Fukushige & Heggie 1995).

The middle column of Figure 3 shows that as the fraction of the disrupted population is increased, the predicted ratio of young to old clusters increases dramatically. The age distribution for cluster populations affected by different levels of infant mortality are shown in Figure 4. The top-middle panel shows that for a constant rate of cluster formation, with *no* disruption, a mass limited cluster sample would have a flat distribution in the  $\log dN/d\tau$  vs.  $\log\tau$  diagram. Higher values of infant mortality would cause steeper age distributions, as shown by the solid points in the next three (middle) panels in Figure 4. The predicted age distributions in Figure 4 are also compared with the empirical age distribution for the Antennae galaxies (presented in Fall et al. 2005). In this figure, it is obvious that the 90% constant number loss (i.e., infant mortality-type disruption) gives the best match between models and observations, although the 80% model is also reasonable given the uncertainties (e.g., the datapoint for the youngest clusters may be artificially high due to a recent burst of star formation in the “overlap” region; see §2.4).

The main shortcoming of this model is that we do not expect it to be relevant past a few  $\times 10^8$  years, at which point two-body relaxation should begin to dominate (Fall et al. 2005). We also note that from an empirical standpoint, the 90 % disruption rate has only been shown to be roughly linear out to about this age (i.e., Figure 2 from Fall et al. 2005). After this point stellar contamination begins to affect the dataset.

The third cluster disruption law (not shown) is a two-stage disruption process, which includes both the constant number loss (infant mortality) and the constant mass loss (two-body relaxation) models. While this two-stage process has been discussed previously (e.g., Fall et al. 2005), this work provides the first detailed application to cluster systems. We note that the resulting disruption law is therefore *mass-independent* for young ages and *mass-dependent* for older ages. This will be our primary tool when building our model for the Antennae, and hence will be described in more detail in §3.2.

The fourth cluster disruption law is described in detail in Boutloukos & Lamers (2003; hereafter BL03). They fit the formula  $t_{dis}(M_{cl}) = t_4^{dis}(M_{cl}/10^4 M_\odot)^{\gamma_{BL}}$ , where  $t_4^{dis}$  is the disruption time for a  $10^4 M_\odot$  cluster and  $\gamma_{BL}$  is  $\approx 0.6$ . The value of  $t_4^{dis}$  is derived based on apparent bends in the  $\log dN/d\tau$  vs.  $\log\tau$  and diagram, which as we shall see, vary dramatically from galaxy to galaxy.

Lamers, Gieles, & Portegies Zwart (2005; hereafter LGPZ05) use this technique to determine a very long characteristic disruption time ( $t_4^{dis} \sim 8 \times 10^9$  yr) for clusters in the SMC. Our simulations for LGPZ05 SMC-type disruption is shown in the upper right panels of Figures 3 and 4. Note that using the LGPZ05 value of the disruption formula results in essentially *no* clusters with  $\gtrsim 10^4 M_\odot$  being disrupted in the SMC. Conversely, LGPZ05 find a very short disruption time for clusters in M51 ( $t_4^{dis} = 70$  Myr), with essentially *all* clusters older than 1 Gyr being disrupted. LGPZ05 interpret this large variation in  $t_4^{dis}$  to be caused by different disruption rates due to differences in the local ambient density (for the clusters which have survived gas removal in the first 10 Myr). However, the  $t_4^{dis}$  derived for M51 clusters is shorter by nearly an order of magnitude than predictions from N-body simulations based on the estimated density of M51 (Lamers et al. 2005). Is it really possible that the disruption laws in these two galaxies could be so different ?

The disruption time derived by LGPZ05 for M33 ( $t_4^{dis} = 6 \times 10^8$  yr) is intermediate between the values given for the SMC and M51. We note that the estimated values of  $t_4^{dis}$  decrease monotonically as a function of distance for the SMC, M33, and M51. This led us to investigate whether the bend in the age and mass diagrams that LGPZ05 use to derive  $t_4^{dis}$  could be an artifact caused by the magnitude threshold (which is typically distance dependent), combined with various selection effects.

In Figure 6 we show the resulting age distributions for an artificial population of clusters formed continuously and subject to a magnitude threshold, with three different mass limits assumed. If a sufficiently high mass limit is chosen, the resulting age distribution is flat as expected, since it is not affected by completeness or disruption of clusters. The diagram also shows that as lower mass limits are used, the resulting age distributions become incomplete due to the magnitude threshold, resulting in an apparent break. *The vertical lines show that the break in the age distribution occurs near the age where the magnitude threshold intersects with the mass limit.* Similar results are found using the infant mortality or two-stage disruption laws, but with sloping  $dN/d\tau$  diagrams.

One prediction of this analysis is that two galaxies at the same distance, observed using similar magnitude thresholds, should result in similar estimates of  $t_{dis}^4$  (i.e., the observational artifacts would result in the same position of the bend). This appears to be the case, since de Grijs & Anders (2006) find the same value of  $\log(t_{dis}^4)$  for the LMC ( $9.9 \pm 0.1$ ) as LGPZ05 found for the SMC ( $9.9 \pm 0.2$ ). We conclude that currently, there is insufficient data to construct a sample of nearby galaxies which cover a range of distances and local densities needed to definitively establish whether the derived  $t_{dis}^4$  timescales result from biases or density.

To test our suspicion that this may be a magnitude threshold bias, we used our Antennae

dataset according to the prescription of BL03. When restricted to dynamic ranges of age and mass where the data are approximately complete, no breaks are seen in the age and mass distributions (i.e. they are smooth power laws). If age and mass distributions are plotted over larger dynamic ranges where we know completeness is an issue, breaks are seen which imply even shorter  $t_{dis}^4$  timescales than found for M51. Hence, in both this case, and in the artificial cluster simulation described above, we know that the apparent breaks are caused by selection effects and incompleteness. We predict that as age and mass distributions become available for other galaxies it will become evident that any apparent breaks are roughly dependent on the depth of the cluster survey (i.e., the distance), and hence caused by an artifact.

#### 2.4. The Need for Rapid Cluster Disruption (i.e., “Infant Mortality”)

The age-luminosity distribution for the constant cluster formation model (with no disruption but with a magnitude threshold; Figure 2c) looks much different than the observed distribution for the Antennae cluster system (Figure 7). Instead of having the highest density of clusters per unit  $\log\tau$  at older ages, the observations have the highest density of young clusters. This is demonstrated more clearly in Figure 2 from Fall et al. (2005). They find that a plot of  $\log(dN/d\tau)$  vs.  $\log\tau$  for the Antennae clusters has a slope that declines with a value  $\approx -1$  out to an age of a few  $\times 10^8$  yrs, rather than being flat, as would be the case for constant cluster formation with no disruption (see Figures 3 and 4). Hence, if the Antennae has had a history of roughly constant cluster formation during this period, clusters must be disrupted at a rate of  $\tau^{-1}$ . It is not possible with the current observations to determine whether the same relationship extends beyond a few  $\times 10^8$  yrs for masses  $\geq 3 \times 10^4 M_\odot$ , due to potential stellar contamination.

The same result is apparent from an examination of Figure 4. Only the 80% and 90% [i.e., slopes of  $-0.7$  and  $-1.0$  in the  $\log(dN/d\tau)$  vs.  $\log\tau$  diagram] infant mortality laws agree with the data. None of the other disruption mechanisms comes close to reproducing the large fraction of observed young clusters.

Perhaps the high density of young clusters is due to a recent burst of cluster formation in the Antennae? This is likely to be true of course, since the galaxies are currently merging and regions like the overlap region have large numbers of very young clusters. However, if we look at each of the WFPC2 chips independently (Figure 8), we find that the  $\log$  luminosity vs.  $\log\tau$  diagrams for all the chips look quite similar, with the largest numbers of clusters always having ages  $< 10^7$  years! Since it is not possible for the galaxy to synchronize a burst of star formation over its entire disk (i.e., assuming a “signal speed” of  $\approx 30$  km

$\text{s}^{-1}$  [Whitmore et al. 1999] requires approximately 500 Myr for one side of the galaxy to communicate with the other side 10 kpc away), we can only conclude that the vast majority of the clusters are being disrupted almost as fast as they form, making it appear that the largest number of clusters is always the youngest.

If one looks closely at Figure 8, or at the corresponding  $\log(dN/d\tau)$  vs.  $\log\tau$  diagram shown in Figure 9, there actually are small differences on the various WFPC2 CCDs due to variations in the local cluster formation histories. For example, the number of clusters at the youngest ages are especially high for the overlap region (pixel values  $< 370$  on WF3; i.e., the dusty overlap region; see Figure 5b from Whitmore et al. 1999), compared to regions where there appears to be less recent formation, (for example, pixel values  $> 370$  on WF3, which is the dust-free region containing several clusters with ages  $> 100$  Myr). However, these are secondary effects; the primary correlation is the rapid decline in the number of clusters as a function of age for all of the CCDs. We will return to this point in §3.2.

This behavior is not confined to mergers and starburst galaxies, such as the Antennae. In typical spiral galaxies (e.g., M51 - Bastian et al. 2005, Figure 10; M83 - Harris et al. 2002; LMC - Hunter et al. 2003; NGC 6745 - de Grijs et al. 2003c; M51 and M101 - Chandar et al. 2006; M33 - Chandar et al. 1999a,b; SMC - Rafelski & Zaritsky 2005), the observational data almost universally show that the density of clusters per unit  $\log\tau$  is roughly constant. The fact that such apparently different galaxies have such similar cluster age distributions is one more demonstration of the universal nature of cluster demographics, and highlights the dominant role cluster disruption appears to play in all galaxies.

The phenomenon of star cluster disruption is not surprising. We are familiar with the process both observationally (e.g., Wielen 1971; Bica et al. 2001; Rockosi et al. 2002) and theoretically (e.g., Fall & Zhang 2001; Vesperini & Zepf 2003; Baumgardt & Makino 2003)). What is surprising is that *massive, compact* clusters, which might be expected to withstand many of the disruption mechanisms which are important for low mass, diffuse clusters (e.g., two-body relaxation), appear to have disruption time scales that are comparable to those of low mass clusters.

In particular, we note that this is dramatically different from the canonical picture for open clusters developed by Wielen (1971), which showed essentially no cluster disruption for the first  $\approx 100$  Myr (see Wielen 1971, Figure 13). However, it does match the recent results from Lada & Lada (2003) for the young embedded clusters in the solar neighborhood, since they find that  $\sim 90\%$  of these clusters are disrupted in the first 10 Myrs.

A natural explanation for this high infant mortality rate is that most of the YMC's may be unbound when they form (or rapidly become unbound), and dissolve on the order of a few

crossing times (e.g., see discussion in Fall et al. 2005). Briefly, the energy and momentum input from massive, young stars to a protocluster are roughly proportional to the number of massive stars, and to its mass. Therefore, such an internal process would be expected to operate roughly independent of cluster mass, and also independent of host galaxy properties.

## 2.5. Selection Effects and Artifacts

A number of selection effects and artifacts must be taken into account before we are able to compare our synthetic data with the observations. The first selection effect is a magnitude threshold, as shown in Figure 2b. As discussed in §2.3, this magnitude threshold, when coupled with the dimming of clusters with age, can cause serious difficulties when attempting to determine mass and age distributions over wide dynamic ranges.

The second effect that we consider is extinction and reddening due to the presence of dust. Dust is most closely associated with very young clusters. This has been modeled by adopting the Mathis (1990) coefficients for the various filters, and a time dependence defined by:  $A_V(\log\tau) = -2.5 \times \log(\tau/\text{yr}) + 18$  [which results in a mean value of  $A_V = 3$  magnitudes at  $\log\tau = 6.0$ ,  $A_V = 1.0$  magnitudes at  $\log\tau \geq 6.8$ , and  $A_V = 0$  magnitudes at  $\log\tau \geq 7.2$ ]. Noise is added by multiplying the  $A_V$  value by a random number from 0 to 1 and then adding a mean value of  $A_V = 0.2$  to represent random foreground dust. The time dependent component is consistent with the extinction distribution  $A_V(\log\tau)$  found for the Antennae by Whitmore & Zhang (2002) and by Mengel et al. (2005). Using other time-dependent extinction laws (e.g., Charlot & Fall 2000) has only minor effects.

The third artifact we include in the model is the effect of systematic errors introduced by our age-dating method. In Figure 7 we show the luminosity versus age diagram for the clusters in the Antennae galaxies (Whitmore et al. 1999), with ages derived using the technique described in Fall et al. (2005). The most prominent example of an age-dating artifact in this figure is the apparent gap in the distribution for clusters with ages in the range  $\log\tau = 7.0 \rightarrow 7.3$  years (i.e., 10 – 20 Myr), which is produced by the onset of the red supergiant phase. During this phase, the integrated cluster colors change so abruptly that the fitted ages, in the presence of observational errors, become degenerate, with a strong tendency to avoid values just above  $10^7$  yr. This “10 Myr artifact” is found in a wide range of data sets where age-dating techniques employing broad-band colors are used (e.g., Fall et al. 2005; Gieles et al. 2005; Harris et al. 2004).

We have modeled biases due to age-dating by simulating clusters with an even distribution in  $\log\tau$  and mass, adding noise to the predicted photometry, and then running the

simulated data through our normal age-dating technique (which is described in Fall et al. 2005). This procedure is sensitive to the prescription used to derive photometric uncertainties and noise for the simulated cluster population. We utilize a procedure similar to that described in Bastian et al. (2005) for estimating the photometric uncertainty as a function of magnitude in all filters, based on the measured photometric uncertainties for the Antennae data. This assumes that the uncertainty in the observed magnitude of a cluster,  $\Delta m$ , depends on the magnitude,  $m$ , as  $\Delta m = 10^{d_1 + d_2 \times m}$ , where the values of  $d_1$  and  $d_2$  are determined empirically for each filter. In addition, we add scatter to the relationship between magnitude and photometric uncertainty to better mimic a real dataset. For the F658N filter, we find that there is larger scatter about this relation for young clusters which have strong  $H\alpha$  emission, and we introduce an additional age-dependent photometric uncertainty for simulated clusters younger than  $\log\tau = 6.8$  yrs in this filter. The resulting input age versus output (i.e., fitted) age is shown in Figure 10, for clusters more massive than  $3 \times 10^4 M_\odot$  (the lower mass limit adopted in Fall et al. 2005). We find that regardless of the mass cut we use (up to  $10^6 M_\odot$ ), the gap in the age range 10 – 20 Myr does not go away.

Note that this appearance contrasts with Figure 2 in Gieles et al. (2005), where the gap appears to be present only at lower masses, but then fills in for higher mass clusters. We suggest that this is due to an underestimate in their models of the true photometric uncertainties at higher masses. As in this work, the Gieles et al. (2005) simulations use the SED models for both the input and output. Hence if the photometric uncertainties are underestimated, the age dating algorithm will always find the “right” answer. In reality, there will be a mismatch between the models and the observations, resulting in a 10 Myr gap at all masses, as seen in the actual data.

Figure 10 allows one to see in more detail where the data from the “gap” is repositioned. While there is a clear, well-defined correlation between the input and output ages, the reason for the 10 Myr artifact can be seen as a repositioning of many of the clusters with ages between  $\log\tau = 7.0$  and 7.2 to an age of  $\log\tau = 7.3$ .

A second prominent feature in Figure 10 is the filled region of points between  $\log\tau$  of 6.0 and 6.4 yrs. This feature implies that clusters with intrinsic ages between 1 and 2.5 Myr cannot be separated using integrated colors and narrow band photometry alone. This is not surprising, given that the  $H\alpha$  emission predicted by models “saturates” at these very young ages, hence we see a large concentration there.

Other potentially important selection effects and artifacts are: limited spatial resolution (i.e., confusion between clusters and stars), blending of objects, and stochasticity for low mass clusters (e.g., below  $10^4 M_\odot$  the chances of having a single O star becomes much less than unity, which can affect the photometric colors dramatically; see e.g., Cervino, Valls-Gabaud,

& Mass-Hesse 2002; Ubeda, Maiz-Apellaniz, Mackenty 2006; Oey & Clarke 1998). These and other effects will be simulated in more detail in future versions of the model.

### 3. Results

Two topics are examined in the current paper in order to exercise the model described in the previous section. The first looks at whether the model can account for the  $M_V(\text{brightest})$  vs.  $\log(N)$  diagram, as shown in Figure 1. The second topic is the development of a toy model for the Antennae galaxies. Paper II will extend the analysis to datasets for a number of other nearby galaxies (e.g., M101, M51, etc.).

#### 3.1. A Monte-Carlo Simulation of the $M_V(\text{brightest})$ vs. Log (N) Diagram

As briefly described in the Introduction, the  $M_V(\text{brightest})$  vs.  $\log(N)$  diagram (Whitmore 2003, originally presented in 2000 as astro-ph/0012546) provided much of the initial impetus for the development of the framework developed in the present paper, since it was consistent with the idea that mergers, starbursts, and normal spiral galaxies all share a common universal power law luminosity function  $\phi(L)$  for clusters. Larsen (2002) further developed this basic idea by performing Monte Carlo simulations of cluster populations. This study supports the conclusion that the magnitude of the brightest cluster is controlled by statistics rather than by physics. Additionally, Larsen (2002) shows that the observed spread in the scatter of the relation can also be explained by statistics. Several other studies have also begun to address the important role this “size-of-sample” effect can play in the observed properties of star cluster systems (e.g., Billet et al. 2002; Hunter et al. 2003; Weidner, Kroupa & Larsen 2004).

Figure 1 shows an updated version of the database from Whitmore (2003). Several more galaxies have been added, primarily from the Larsen (2005) compilation, and the values have been updated for individual galaxies where more recent work has become available.

Here, we present a test of the power law index  $\alpha$  over absolute magnitudes ranging from  $M_V$  of  $-9$  to  $\sim -16.5$ . Figure 11 shows a comparison between the observational data presented in Figure 1 with sets of Monte-Carlo simulations of 500 cluster populations, which are randomly drawn from a power law luminosity function with values of the index  $\alpha$  ranging from  $-1.5$  to  $-3.0$  and ages between 1 and 100 Myr (i.e., the brightest clusters are essentially always found in this age range). The 90 % infant mortality law is assumed for this particular simulation. Several other star formation histories have also been tested (e.g., constant with



time, Gaussian bursts at various times) with similar results. An observational cutoff brighter than  $M_V = -9$  has been imposed on both the observations and the simulations.

The figure shows that values of  $\alpha$  equal to  $-1.5$  and  $-3.0$  are clearly ruled out. Values of  $\alpha$  between  $-2.0$  and  $-2.4$  all fit the observations to some degree, with values of  $-2.0$  matching the slope, but showing an offset of about 1 magnitude, and values around  $-2.4$  showing no offset, but having a flatter slope than the observations. Values of the fits are included in Table 1. It is likely that part of the offset is due to many of the datasets not being complete to  $M_V = -9$ ; hence the value of the number of clusters in the sample,  $N$ , is underestimated. In principle, the slope  $\alpha$  should only reflect the underlying luminosity function. However, different selection effects (such as the imposed cutoff of  $M_V = -9$ ), can affect the measured slope. For this reason, we consider the  $\alpha = -2.2$  fit as the best compromise between matching the slope and minimizing the offset, and estimate an uncertainty of 0.2.

Figure 12 shows a comparison between the scatter in the observations and the simulation for our adopted  $\alpha = -2.2$  model. Based on the similarities between the two, we conclude, as Larsen (2002) did, that the observational scatter can be explained just by statistics. There is no indication that any “special physics” is needed to explain the differences between, for example, the cluster systems of mergers and spiral galaxies.

We conclude that both the correlation between  $M_V(\text{brightest})$  and  $\log(N)$  and the scatter in the correlation can be explained by statistics if all star forming galaxies have the same universal initial luminosity function. The only difference is the normalization, with mergers having thousands of clusters brighter than  $M_V = -9$ , and spirals having tens of such clusters. One possibility for the much larger number of clusters in mergers is that the conditions for making young massive clusters are *globally* present while in spiral galaxies they are only *locally* present (i.e., in the spiral arms; Whitmore 2003).

## 3.2. A Model of the Antennae

### 3.2.1. Background

Because of its proximity (19.2 Mpc), large collection of young massive clusters, and extensive set of multi-wavelength observations (e.g., Zhang, Fall & Whitmore 2001), the prototypical merger NGC 4038/4039 (the “Antennae”) currently represents the best dataset for testing the model described in this paper. Here, we briefly summarize the observations and analysis from these previous works.

The *HST* observations of the Antennae galaxies are described more fully by Whitmore

et al. (1999). The images were taken in 1996 January by the Wide-Field Planetary Camera 2 (WFPC2) with each of the broadband filters F336W (*U*), F439W (*B*), F555W (*V*), and F814W (*I*), and with the narrowband F658N (*H $\alpha$* ) filter. Approximately 14,000 point-like objects (stars and clusters) were detected.

We estimate both the age ( $\tau$ ) and extinction ( $A_V$ ) of each cluster by comparing the observed magnitudes in the five bands with those from stellar population models, as described in Fall et al. (2005). More specifically, we use the Bruzual & Charlot (2003) models with solar metallicity and Salpeter IMF. While this metallicity is appropriate for comparison with young stellar populations ( $\lesssim 1$  Gyr), estimates of ages for older stellar populations should be viewed with caution, as they suffer from the well-known age-metallicity degeneracy, and likely have abundances lower than the solar value. Because dust is prevalent and patchy, it is important to estimate the internal effects of dust individually for each cluster. However, for compact star clusters in dusty regions it is not obvious that either a simple foreground screen or an attenuation law which assumes gas and dust mixed with stars (e.g., Calzetti, Kinney & Storchi-Bergmann 1994) is appropriate. We therefore experimented with both a Galactic-type extinction law (Fitzpatrick 1999) and the absorption curves determined from starburst galaxies by Calzetti et al. (1994) for the age dating procedure. The main difference between the two is the value of  $R_v$ , which is 3.1 for Galactic extinction laws and 4.05 for the Calzetti absorption law. We found relatively minor differences in the results, with little change in the derived cluster ages, and masses which were 10 – 20% higher for clusters younger than  $10^7$  yrs when the Calzetti law was assumed.

As briefly described in the Introduction, our earlier analysis of the Antennae dataset provided some of the motivation for the current paper. Of particular relevance for the current work, Fall (2006) notes that the mass and age distributions over limited ranges for the Antennae cluster system are *independent* of one another. This means that the joint distribution  $g(M, \tau)$  must be the product of the mass and age distributions,  $\psi(M)$  and  $\chi(\tau)$ , which roughly follow the relation:

$$g(M, \tau) \propto M^\beta \tau^\gamma \propto M^{-2} \tau^{-1} \quad \text{for } \tau \lesssim 10^7 (M/10^4 M_\odot)^{1.3} \text{ yr} \quad (1)$$

as used in §2 to define the approximate mass–age distributions of the massive young clusters.

In general the luminosity function is *not* independent of the mass and age distributions. However, under certain circumstances (e.g., when the mass distribution is a power law and is independent of the age distribution) the luminosity and mass functions can both be power laws with the same exponent. This appears to be the case for the Antennae, with  $\phi(L)dL \propto L^\alpha dL$ ; and  $\alpha \approx -2$  for  $-14 < M_V < -6$  (Whitmore & Schweizer 1995; Whitmore et al.

1999), and  $\psi(M)dM \propto M^\beta dM$ , with  $\beta \approx -2$  for  $10^4 - 10^6 M_\odot$  (e.g., Zhang & Fall 1999; Fall, Chandar, & Whitmore 2006).

Our purpose here is not to revise the previous work, but rather to extrapolate to both higher and lower mass ranges. Applying these relations, the model allows us to take the next step and move beyond the observed cluster system, and compare predictions with the integrated properties of a galaxy (e.g., the total stellar mass and total luminosity). For example, to the degree that our models fit the integrated galaxy properties, we can have some confidence that extrapolations outside of the original age and mass ranges (as specified in equation 1) are reasonable.

In addition, we can test a variety of the other assumptions that go into the model. Does our assumption that all stars form in clusters, and that the field stars are the remnants of disrupted clusters, give values for the luminosities of the clusters and field which are consistent with observation? Can we predict other distributions (or different projections of the data, e.g., color-color and color-magnitude diagrams) which were not used in the original determination of  $\alpha$ ,  $\beta$ , and  $\gamma$  above? Does an extrapolation to the highest observed mass support the recent suggestion that the Antennae system has a fixed upper cluster mass? While there is already some evidence that parts of the model are consistent with observations for a few other nearby galaxies (see, for example, §1 and Figures 1, 11, 12, 15), in Paper 2 we will extend the analysis to a larger sample to better test the universality of the basic framework.

### 3.2.2. 4-Component Model of the Antennae

We begin by constructing a model for the Antennae which assumes four cluster formation components, which are derived from previous information (Whitmore et al. 1999). The four components are as follows: Component # 1 - An initial Gaussian burst with an age of 13 Gyr and  $\sigma$  of 1 Gyr that formed the population of old globular clusters. Component # 2 - A constant rate of cluster formation over the past 12 Gyr similar to the cluster formation rate in typical spiral galaxies. Component # 3 - A Gaussian burst of cluster formation  $500 \pm 100$  Myr ago that was triggered when the galaxies first encountered each other and the long tidal tails were ejected. Component # 4 - An increased rate of cluster formation during the past 100 Myr responsible for most of the recent star/cluster formation. The last two components are also motivated by the simulations of the dynamical interaction between the two galaxies (Barnes 1988), which suggested that the galaxies first encountered each other a few 100 Myr ago, and are now in their second encounter. *Hence, the 4-component model essentially has no free parameters.* It is an attempt to construct a model using previous determinations of

$\beta$ ,  $\gamma$ , and the cluster formation history of the Antennae, and an assumption that the power laws continue beyond the ranges where they have been observed directly.

The observations and derived properties of the Antennae are shown in the left column of panels in Figure 13. In order to restrict the Antennae sample to actual star clusters and not individual stars, we make a cut in absolute luminosity at  $M_V = -9$  (see Whitmore et al. 1999). Following Fall et al. (2005), we also impose a mass limit ( $\geq 3 \times 10^4 M_\odot$ ). Note that in the age versus mass figure of the Antennae clusters this mass limit begins to show incompleteness for clusters starting at ages  $\sim 10^8$  years.

The model uses a value of  $\beta = -2.0$  and the two-stage disruption law with 90 % infant mortality, as motivated above. This 4-component Antennae model is shown in the middle column of Figure 13. We remind readers that the apparent gap in the age distribution around 10 Myr (i.e., Figures 7 and 10) is due to artifacts from the age-dating algorithm. While our modeling of this artifact (§2.5) is able to subjectively reproduce the major features, some of the small-scale remaining differences (e.g., the narrowness of the 10 Myr artifact) are still not very well represented.

There is reasonable agreement between the 4-component model and many of the diagnostics and observations (e.g., the  $\log(dN/d\tau)$  vs.  $\log\tau$  diagram) right out of the box (i.e., using previous determinations of  $\beta$ ,  $\gamma$ , and the cluster formation history of the Antennae). However, a closer look reveals three issues: 1) the lack of intermediate-age clusters around 100 – 300 Myr (besides being evident in the luminosity-age and mass-age diagram, this deficit can also be seen in the color-color diagram as the slight misplacement of the small enhancement around  $U - B = 0.0$  and  $V - I = 0.5$  mag; see also Figure 17 from Whitmore et al. 1999); 2) a slight deficit in the number of young clusters with ages 1 – 10 Myr; and 3) a slight enhancement in the predicted number of very luminous and/or very massive clusters.

The first difference can be fixed if we move the 500 Myr burst to an age of about 200 Myr. There is independent evidence for this in the numerical modeling of the Antennae (Barnes 1988). The second difference is the need for an enhancement at very young ages (i.e., 1 – 10 Myr). This is probably related to the enhancement we see in the overlap region (on WF3 as already noted in §2.4). The third difference suggests either the possibility of an upper mass cutoff for the clusters, or a slightly steeper initial mass function (i.e.,  $\beta = -2.1$  rather than  $-2.0$ ; these possibilities are explored in §3.3).

### 3.2.3. 5-Component Model of the Antennae

Our second attempt at making a model takes into account the shortcomings of the 4-component model mentioned above. Because of the addition of a 1 – 10 Myr component (to address the second shortcoming), we now refer to this as the 5-component model. In addition, we relax the constraint that only the canonical values of  $\gamma = -1$  (i.e., the coefficient describing the infant mortality law) and  $\beta = -2.0$  must be used.

The 4-component model had a total galaxy luminosity that is considerably too high (i.e.,  $M_{V,galaxy} = -23.0$ , compared with the estimated  $M_{V,galaxy} = -21.7$  for the Antennae; Whitmore et al. 1999). We therefore used an 80 % infant mortality law (i.e.,  $\gamma = -0.7$ ) for all components of our 5-component Antennae model which results in a smaller total galaxy luminosity and mass. This is because the predicted cluster population is normalized to the observed Antennae cluster system, so that the lower rate of cluster disruption implies that fewer clusters were formed initially. This also creates a smaller number of very young clusters, which is accounted for by increasing the 1 – 10 Myr component slightly. From Figure 4 it appears that the 80% and 90% infant mortality laws both give reasonable fits. Finally, we change the power law mass index  $\beta$ , from  $-2.0$  to  $-2.1$ , as justified in §3.3. These two changes reduce the total galaxy mass to  $\sim 4 \times 10^{10} M_{\odot}$  and total  $M_{V,galaxy}$  to  $-22.2$  (much closer to the observed value of  $-21.7$ ; see Table 2). The results from the final 5-component model are shown in the right column of Figure 13.

As an additional consistency check, we compare the predicted UV luminosity in clusters from our 5-component model with the observed luminosity. The model predicts that  $\sim 7\%$  of the UV luminosity should come from clusters. This is quite similar to the value of  $\sim 9\%$  measured for the Antennae cluster system by Whitmore & Zhang (2002).

While we could have continued to tweak various parameters in our model to exactly match the observations of the Antennae, we do not think this approach is useful, since there are a large number of potential variables, many of them coupled. Instead, our approach has been to only make changes where there is an independent indication that a value should be changed (e.g., the 500 Myr component should be changed to 200 Myr; see previous section). The only exceptions are the variables  $\beta$  and  $\gamma$ , which we allowed to vary (within the uncertainties) in order to address the discrepancy between the predicted and observed total galaxy mass and luminosity.

### 3.3. Is There an Upper Mass Cutoff for Clusters in the Antennae?

Is there a physical limit with which star clusters in the Antennae can form, or does the most massive cluster just result from statistics? Gieles et al. (2006) have suggested that the former is true in the Antennae. In §2.2 and §3.1, we showed how the maximum cluster mass increases with the total number of clusters. Given its very rich population of clusters, the Antennae is an ideal galaxy to test whether there is any evidence for a physical upper mass cutoff with which clusters can form.

As briefly noted in §3.1, the cluster luminosity function for the 4-component Antennae model (shown in the middle column in Figure 13) agrees quite well with the data for the fainter magnitudes, but the simulations slightly overpredict the number of the brightest clusters. This results in an observed luminosity function which is too flat, especially at the bright end.

To explore the possibility of a cutoff to the cluster mass function, we started with a slope  $\beta \sim 2.0$  model, which is known to hold for young  $10^4 - 10^6 M_\odot$  clusters in the Antennae (Fall, Chandar, & Whitmore 2006). Because the high mass end of the cluster mass function suffers from small number statistics the total number of clusters,  $N$ , used for each realization was determined empirically (by matching the simulation to the observed number of Antennae clusters with masses between  $5 \times 10^4 M_\odot$  and  $5 \times 10^5 M_\odot$ ). The number of predicted clusters with masses  $> 10^6 M_\odot$  was then compared with the observed masses of clusters in the Antennae.

Figure 14 shows the result from our Monte-Carlo simulations. The left column shows a comparison of the Antennae values (dashed line) for the brightest, 3rd brightest, and 10th brightest cluster with similar ranked clusters from the simulations for  $\beta = -2.0$ . There does appear to be a difference between the simulations and data, with the simulations predicting somewhat larger masses (i.e., at the  $1 - 2 \sigma$  level) for all three panels. However, we note from Figure 14 that this might also be explained by a small difference in the value of  $\beta$ . Simulations showing the results assuming  $\beta = -2.1$  and  $\beta = -2.2$  are shown in the middle and right panels respectively.

Figure 14 shows an asymmetric tail toward larger masses for all tested values of  $\beta$ , predicting that in a few cases, cluster masses as high as  $10^8 M_\odot$  or even (very rarely)  $10^9 M_\odot$  might be expected if there is no upper mass cutoff. This high mass tail might explain the existence of W3 in NGC 7252, which has a dynamical mass  $8 \pm 2 \times 10^7 M_\odot$  (Maraston et al. 2004).

For the Antennae, our sample contains a number of clusters more massive than the proposed limit of  $1.9 \pm 0.6 \times 10^6 M_\odot$  suggested by Gieles et al. (2006). In fact the  $\beta = -2.1$

simulation in particular provides a good match to observed cluster masses  $\geq 10^6 M_\odot$  in the Antennae, and is within the observational uncertainties for the mass function measured for young clusters in this galaxy. Hence, we find that the cluster mass distribution in the Antennae galaxies *does not require* a truncation at the high mass end, and can be explained by sampling statistics and an initial mass function slope  $\beta \sim -2.1$ . Note however, that the small number of very massive clusters in our sample results in large uncertainties at this end of the cluster mass function. Therefore the current observations cannot exclude an actual cutoff in the Antennae mass function above  $\sim \text{few} \times 10^7 M_\odot$ .

## 4. Discussion

### 4.1. Potential Anomalies and Predictions

We have demonstrated that our framework and simple toy model can explain the basic demographics of star clusters in the Antennae galaxies, and in Paper 2 we will show that the same framework can be used to successfully model other nearby galaxies. However, it is possible to think of apparent exceptions to the framework outlined above.

One example of a potential anomaly, the very bright cluster in NGC 1569, has already been discussed extensively in the literature (e.g., Whitmore 2003; Billet et al. 2002; Larsen 2002). We first note that this cluster is no longer as discrepant as previously believed, since the number of detected clusters in the sample of Hunter et al. (2000) ( $N = 18$  with  $M_V < -9$ ) is larger than in the original study by de Marchi et al. (1997) ( $N = 7$ ). In §3.1 we found that the scatter predicted by statistics is consistent with the observed scatter. The position of NGC 1569 in Figure 1 using the new Hunter data is  $\lesssim 2\sigma$  (predicted scatter) from the mean relation. Hence the point is no longer very discrepant.

We should, however, keep in mind that subtle selection effects can alter the results for individual galaxies. For example, Billett et al. (2002) and Whitmore (2004) both point out that in a sample of star forming dwarf galaxies, the ones with the brightest clusters (i.e. the  $1 - 2 \sigma$  high points) are more likely to have drawn attention to themselves and to have been observed than dwarf galaxies that have not formed bright clusters (i.e., the  $1 - 2 \sigma$  low points).

The second apparent anomaly we discuss is the lack of intermediate-age globular clusters in the Milky Way. If the majority of stars form in clusters, and the initial cluster mass function is universal, then the fact that there are many intermediate-age stars (for example the Sun !), implies that there should be some intermediate-age (i.e., a few billion year old) globular clusters.

To some extent this may just be a matter of semantics. The tail of the distribution of old “open” clusters may simply be intermediate-age globular clusters, as suggested in Whitmore (2003). While there are only a handful of known old open clusters, we should keep in mind that the catalogs of open clusters are only complete within a distance of about 1 – 2 kpc of the sun; hence the volume for the entire Milky Way is roughly 100 times larger. There are certain to be many more clusters in this category hidden behind the dust in the plane of the Milky Way. Indeed, in neighboring spiral galaxies, where we are able to see the entire disk, intermediate-age globular clusters are now being found (e.g., in M31 see Puzia, Perrett, & Bridges 2005; Beasley et al. 2004; Burstein et al. 2004; Li & Burstein 2003; Barmby & Huchra 2000; but see Cohen et al. 2005 concerning the inclusion of asterisms in some of these compilations; in M33 see e.g., Chandar et al. 2002, 2006).

We might also note that due to a combination of the various disruption mechanisms and the completeness limit, the number of observable intermediate-age clusters is expected to be relatively low. For example, in our 5-component simulation of the Antennae, only  $\sim 10$  clusters are predicted in the range 1 – 10 Gyr with  $M_V > -9$ , and only 8 clusters are observed in this region. The excess of clusters with ages  $\approx 13$  Gyr (i.e., old globular clusters) in the model and in the data is due to a strong initial burst, which is expected to produce roughly the same number of clusters as are produced in the next  $\approx 10$  Gyr.

The third “anomaly” that we address is the apparent difference between the metallicity distribution of Galactic field stars, with a broad peak around  $[\text{Fe}/\text{H}] \approx -0.8$ , and the metallicity distribution of the globular clusters, which is bimodal with peaks around  $[\text{Fe}/\text{H}] \approx -1.3$  and  $-0.75$  for the Galaxy (see Figure 8 in Cote 1999). This is highlighted in Harris (2003) for M31, and by Beasley et al. (2003) for NGC 5128. In the simplest version of our model, we would predict that the metallicity distributions of the field stars and the clusters would be identical.

Harris (2003) points out that another way of thinking about this is that the specific frequency (number of clusters per galaxy luminosity) needs to be roughly 5 times larger for the blue (metal-poor) clusters than the red (metal-rich) clusters. He argues that the efficiency of *formation* of the blue clusters must somehow be higher. However, another possibility is that the difference lies in *disruption* rather than formation mechanisms. In the context of the current paper, this might simply be explained by changing the infant mortality rate from 90 % for the current epoch to 80 % during the epoch when the old (blue) globular cluster population formed. This would result in  $\sim 4$  times more blue clusters surviving infant mortality in the first 100 Myr. Hence, a very small change in the survival rate for the blue, metal-poor clusters would be enough to change the value of  $S_N$  by a factor of  $\approx 5$  without significantly changing the overall framework of the model. We refer the reader to Harris et



al. (2006) for a discussion of what might cause the blue, metal-poor globular clusters to have a lower disruption rate. More generally, any correlated variable (for e.g., orbital motions), which correlates with metallicity and also couples to disruption rates would achieve a similar result (see Fall & Rees 1985 for a discussion of this point). This topic will be addressed more carefully in Paper II.

#### 4.2. Choice of the Initial Cluster Mass Function

In this paper, we have assumed a single power law for the initial mass function, since many works point to this form (see references in the Introduction). However, recently there have been suggestions that the initial mass function may be a broken power law (e.g., Mengel et al. 2005; Gieles et al. 2006) or even a Gaussian (e.g., Fritze-van Alvensleben 2004; de Grijs, Parmentier, & Lamers 2005). A full treatment of these forms is beyond the scope of this work, particularly since in our judgement, there are a number of reasons to remain suspicious of these suggestions.

Mengel et al. (2005) present a cluster mass function for the Antennae which is best fit by two power laws or a “broken” power law (i.e., the mass function is steeper at the high mass end, and flattens towards lower masses). They use a K-band limited cluster sample, which is much shallower than the *HST* data referred to here. As they make clear, their sample selection has very complicated and poorly understood selection effects, making it difficult to assess incompleteness, and likely affecting the low mass end of their mass function. Given these difficulties, Mengel et al. (2005) caution against “over-interpreting” the presentation of their mass function. A comparison of the Antennae mass function discussed in §3.3 and that presented in Mengel et al. (2005) shows good agreement in the slope at the high mass end (see Fall et al. 2006). Their mass function begins to deviate (becomes shallower) from ours at lower masses, exactly as expected from a shallower data set without robust completeness corrections.

De Grijs, Parmentier, & Lamers (2005) claim that the mass function for the 1 Gyr cluster population in M82 was initially a Gaussian, and that there has been essentially no disruption of low mass clusters in this galaxy. They find that the mean mass they derive for the 1 Gyr population is  $\approx 10^5 M_{\odot}$ , essentially the same as a normal population of old globular clusters. Hence, they argue, there is no room for the disruption of low mass clusters if this population is to evolve into a classic globular cluster system in  $\sim 10$  Gyr. However, we note that this conclusion is not consistent with their own data, since all nine of the clusters with ages less than 100 Myr in Figure 3 of de Grijs et al. (2003a) have masses less than  $10^5 M_{\odot}$ . Given the high and variable extinction in this galaxy, we suspect that completeness

and extinction effects may be underestimated for their 1 Gyr population, resulting in an overestimate of the mean mass of the population.

We conclude by noting that in the Antennae at least, clusters with masses less than  $\approx 10^8 M_\odot$  and ages less than 100 Myr clearly have a power law mass distribution down to the limit where clusters can be separated from stars based on luminosity (Zhang & Fall 1999; Fall 2004; Fall et al. 2006), hence justifying our assumption of an initial power law mass function in our model.

#### 4.3. The Antennae as a Scaled-Up Version of the Milky Way

Lada & Lada (2003) make several of the same points about the need for rapid cluster disruption for very young clusters in the Milky Way, that are made for the Antennae in this paper (§3.2). In fact, it is possible to view the cluster demographics in the Antennae as a scaled-up version of the Milky Way. According to Lada & Lada (2003), the Milky Way has roughly 100 known embedded young clusters within a distance of  $\approx 1$  kpc. The most massive clusters in their sample are slightly more massive than  $10^3 M_\odot$ . If we were able to see the entire disk of the Milky Way the sample would be roughly 100 times larger. The current star formation rate per unit area in the Antennae is also roughly a factor of 10 higher than the Milky Way (Zhang, Fall, & Whitmore 2003), hence the total enhancement for the number of young clusters in the sample might be roughly a factor of 1000. Assuming a universal power law with index  $\approx -2$  for the initial mass function, the most massive clusters with comparable ages to the Lada & Lada sample (i.e.,  $\approx 10$  Myr) would be predicted to be slightly more massive than  $10^6 M_\odot$ , just as they are in the Antennae.

Lamers et al. (2005) have used the new catalog of Galactic open clusters from Kharchenko et al. (2005) with the predictions of the BL03 cluster disruption model. They find an apparent break in the  $dN/d\tau$  diagram around  $\log\tau = 8.5$  yrs, and interpret this in the context of their model (see §2.3 for a discussion) as evidence for a value of  $t_4^{dis} = 1.3 \pm 0.5$  Gyr. However, if we add the embedded clusters from Lada & Lada (2003) to their sample, most or all of the evidence for a bend in the  $dN/d\tau$  diagram goes away. Hence, the Lamers et al. (2005) result for the Galactic open cluster  $t_4^{dis}$  may be another example where selection effects and sample incompleteness (i.e., not including the young embedded clusters from Lada & Lada 2003) can produce an apparent bend in the age distribution, which can be misinterpreted in the BL03 models as evidence for a specific value of the “disruption time”.

In Figure 15 we plot cluster age distributions for the Lada & Lada (2003) embedded cluster sample, the Kharchenko et al. (2005) open cluster sample, and our Antennae clusters

more massive than  $10^5 M_\odot$ . In addition, we show the age distribution for clusters in the SMC using data from Rafelski & Zaritsky (2005), but reinterpreted by Chandar, Fall & Whitmore (2006). We note that a  $dN/d\tau \propto \tau^{-1}$  dependence again fits the data, although Rafelski & Zaritsky (2005) quote a power law fit to this distribution of  $dN/d\tau \propto \tau^{-2}$  in their paper (see discussion in Chandar, Fall & Whitmore 2006).

To summarize, Figure 15 shows that the cluster age distribution in these three very different environments (and covering different mass ranges) all exhibit the same characteristic behavior, with a  $\sim \tau^{-1}$  decline in the number of clusters with age over the first  $\sim 10^9$  years.

## 5. SUMMARY

Motivated by our previous results using age and mass distributions for the Antennae cluster system, and similar results for a few other galaxies, we have developed a framework for understanding the demographics of star clusters, along with a toy model. This model incorporates a universal initial power law mass function, selected formation histories, selected disruption mechanisms, and a convolution with artifacts and selection effects. The three key parameters in the models are the power law index for the mass function ( $\beta \approx -2$ ; primarily affects the cluster mass distribution at the high mass end and total galaxy mass and luminosity), the percentage of clusters disrupted in the infant mortality disruption law ( $\approx 90$  % per decade of  $\tau$ ; i.e.,  $\tau^{-1.0}$  dependencies; primarily affects the total galaxy mass), and the mass loss rate  $\mu_{ev}$  (primarily affects the shape of the observed cluster mass function and the total mass).

A wide variety of observations can be explained by this simple model. In this particular contribution we concentrate on the  $M_V(\text{brightest})$  vs.  $\log(N)$  relationship and on extending the range of comparison for observations of the Antennae galaxies. In Paper II we consider several other nearby galaxies.

1. The correlation between the brightest young cluster in a galaxy and the total number of young clusters [i.e.,  $M_V(\text{brightest})$  vs.  $\log(N)$ ] can be understood as a statistical size-of-sample effect rather than a difference in the physical process responsible for the formation of the clusters. One possibility for the much larger number of clusters in mergers is that conditions for making young massive clusters are globally present while in spiral galaxies they are only locally present (i.e., in the spiral arms). The diagram is quite sensitive to the value of  $\alpha$  for the initial power law luminosity function, with relatively good agreement in the range  $-2.0 < \alpha < -2.4$ .

2. A detailed comparison is made between different cluster disruption laws and it is

demonstrated that the apparent break in the  $dN/d\tau$  vs.  $\log\tau$  diagram used to determine the parameters in the Boutloukos & Lamers (2003) model may be produced by incompleteness at the breakpoint.

3. A 4-component model of the Antennae galaxies was first developed using only pre-existing information (i.e., 90 % infant mortality rate,  $\beta = -2.0$ , and cluster formation histories from Whitmore et al. 1999). The model showed reasonably good agreement with the data, although there were three minor areas of disagreement. In addition, the total magnitude predicted for the galaxy by extrapolating  $\beta$  to the low stellar mass regime was  $\approx 1$  magnitude brighter than the Antennae.

These shortcomings were addressed in a 5-component model of the Antennae galaxies which agrees with the observations quite well, based on matches to the magnitude-age, number-magnitude (i.e., luminosity function), color-magnitude, color-color, mass-age and number-age (i.e., age distribution) diagrams. The model employs a two-stage cluster disruption law with 80% infant mortality in the first 100 Myr (i.e., a  $\gamma \approx -0.7$  dependence; similar to the observed value of  $\gamma \approx -1$ ; Fall et al. 2005), and a value of  $\beta = -2.1$  for the index of the initial mass function (within the uncertainties of previous studies, which were determined directly over a more limited age-mass domain; Zhang & Fall 1999; Fall 2004; Fall et al. 2006). This results in a predicted total galaxy mass and luminosity, and fraction of UV light in clusters, that are in reasonably good agreement with the observations (see Table 2).

4. We find no evidence for a truncation of the cluster mass function at the high mass end. In fact,  $\beta \sim -2.1$  gives a good match to the observed cluster mass function above the stellar contamination limit (see Fall et al. 2006 for a more detailed treatment).

5. Four potential anomalies are examined and found not to be serious problems for the framework. The brightest cluster in NGC 1569 falls well within the statistical uncertainty expected by the model. Intermediate-age globular clusters have recently been found in nearby spiral galaxies such as M33 (e.g., Chandar et al. 2002; 2006) and M31 (e.g., Barmby & Huchra 2000; Li & Burstein 2003; and Puzia et al. 2005). The difference in the metallicity [Fe/H] distribution functions of stars and globular clusters in various galaxies may be due to less effective disruption of the metal-poor clusters (e.g., Fall & Rees 1985; Harris et al. 2006). The claim by de Grijs et al. (2005) that the initial mass function in M82 is a Gaussian is not consistent with their own data for the young clusters, and is clearly not the case in the Antennae (Fall et al. 2006).

6. It is demonstrated that the basic demographics of the star clusters in the Antennae galaxies are consistent with a “scaled-up” version of the local neighborhood of the Milky

Way. The required scaling factor ( $\approx 1000$ ) is due to the larger volume and higher star formation rate in the Antennae. This provides general support for the universal nature of the framework outlined in this paper.

We thank Francois Schweizer and the referee for comments which improved the paper. This work was partially supported by NASA grants GO-09720-A and GO-10188-A. *HST* data are obtained at STScI, which is operated by AURA, Inc., under NASA contract NAS5-26555.

## REFERENCES

- Applegate, J. H. 1986, *ApJ*, 301, 132
- Ashman, K., & Zepf, S. 1998, *Globular Cluster Systems* (Cambridge: Cambridge University Press)
- Barmby, P., Huchra, J. P., Brodie, J. P., et al. 2000, *AJ*, 119, 727
- Barth, A.J., Ho, L. C., Filippenko, A. V., & Sargent, W. L. 1995, *AJ*, 110, 1009
- Barnes, J. 1988, *ApJ*, 331, 699
- Bastian, N., Gieles, M., Lamers, H.J.G.L.M., Scheepmaker, R.A., & de Grijs, R. *A&A*, 2005, *A&A*, 431, 905
- Baumgardt, H., & Makino, J. 2003, *MNRAS*, 340, 227
- Beasley, M. A., Brodie, J. P., Strader, J., et al. 2004, *AJ*, 128, 1623
- Beasley, M. A., Harris, W. E., Harris, G. L., & Forbes, D. A. 2003, *MNRAS*, 340, 341
- Bica, E., Santiago, B. X., Dutra, C. M., Dottori, H., de Oliveira, M. R., & Pavani, D. 2001, *A & A*, 366, 827
- Billett, O. H., Hunter, D. A., & Elmegreen, B. G. 2002, *AJ*, 123, 1454
- Boily, C. M. & Kroupa, P. 2003a, *MNRAS*, 338, 665
- Boily, C. M. & Kroupa, P. 2003b, *MNRAS*, 338, 673
- Boutloukos, S. G., & Lamers, H. J. G. L. M. 2003, *MNRAS*, 338, 717 (BL03)
- Bruzual A. G., & Charlot, S. 2003, *MNRAS*, 344, 1000
- Burstein, D., Li, Y., Freeman, K. C., et al. 2004, 614, 158.
- Calzetti, D., Kinney, A. L., & Storchi-Bergmann, T. 1994, *ApJ*, 429, 582
- Cervino, M., Valls-Gabaud, D., Luridiana, V., & Mas-Hesse, J. M. 2002, *A & A*, 381, 51
- Chandar, R., Bianchi, L., & Ford, H. C. 1999a, *ApJS*, 122, 431
- Chandar, R., Bianchi, L., & Ford, H. C. 1999b, *ApJ*, 517, 668
- Chandar, R., Bianchi, L., Ford, H. C., & Sarajedini, A. 2002, *ApJ*, 564, 712
- Chandar, R., Fall, S. M., & Whitmore, B. C. 2006, *ApJL*, in press (astro-ph/0609360)
- Chandar, R., Puzia, T. H., Sarajedini, A., & Goudfrooij, P. 2006, *ApJ*, 646, L107
- Chandar, R., & Whitmore, B. C. 2006 (in preparation: Paper 2)
- Charlot, S., & Fall, S. M. 2000, *ApJ*, 539, 718
- Chernoff, D. F. & Weinberg, M. D. 1990, *ApJ*, 351, 121

- Cohen, J. G., Matthews, K., & Cameron, P. B. 2005, *ApJ*, 634, L45
- Cote, P. 1999, *AJ*, 118, 406
- de Grijs, R., & Anders, P. 2006, *MNRAS*, 366, 295
- de Grijs, R., Anders, P., Bastian, N., Lynds, R., Lamers, H. J. G. L. M., & O’Neal 2003c, *MNRAS*, 343, 1285
- de Grijs, R., Parmentier, G., & Lamers, H. J. G. L. M. 2005, *MNRAS*, 364, 1054
- de Grijs, R., Bastian, N., & Lamers, H.J.G.L.M. 2003a, *MNRAS*, 340, 197
- de Grijs, R., Bastian, N., & Lamers, H.J.G.L.M. 2003b, *AJ*, 583, L17
- de Marchi, G., Clampin, M., Greggio, L., Leitherer, C., Nota, A., & Tosi, M. 1997, *ApJ*, 479, L27
- Fall, S. M 2006, *ApJ*, in press [astro-ph/0609201]
- Fall, S. M., Chandar, R., & Whitmore, B. C. 2005, *ApJ*, 631, L133
- Fall, S. M, Chandar, R., & Whitmore, B. C. 2006 in preparation
- Fall, S. M., & Rees, M. J. 1977, *MNRAS*, 181, 37
- Fall, S. M., & Rees, M. J. 1985, *ApJ*, 298, 18
- Fall, S. M., & Zhang, Q., 2001, *ApJ*, 561, 751
- Fall, S. M. 2004, in ASP Conf. Ser. 322, “The Formation and Evolution of Massive Young Star Clusters”, ed. H. J. G. L. M. Lamers, L. J. Smith, & A. Nota (San Francisco: ASP), 399
- Figer, D. F., Kim, S. S., Morris, M., Serabyn, E., Rich, R. M., & McLean, I. S. 1999, *ApJ*, 525, 750
- Fitzpatrick, E. L 1999, *PASP*, 111, 63
- Fritze-van Alvensleben, U. 2004, in “Starbursts from 30 Doradus to Lyman Break Galaxies”, eds. R. de Grijs, R. M. Gonzalez Delgado, *Astrophysics & Space Science Library Series*, (Dordrecht: Kluwer)
- Fukushige, T., & Heggie, D. C. 1995, *MNRAS*, 276, 206
- Gieles, M., Bastian, N., Lamers, H. J. G. L. M., & Mout, J. N. 2005, *A & A*, 441, 949
- Gieles, M., Larsen, S., Bastian, N., & Stein, I. 2006, *A & A*, 450, 129
- Harris, J., Calzetti, D., Gallagher III, J. S., Conselice, C. J., & Smith, D. A. 2002, *AJ*, 122, 3046
- Harris, J., Calzetti, D., Gallagher III, J. S., Conselice, C. J., & Smith, D. 2004, *ApJ* 603, 503

- Harris, J., & Zaritsky, D. 2004, *AJ*, 127, 1531
- Harris, W. E., Whitmore, B. C., Karakla, D., Okon, W., Baum, W. A., Hanes, D. A., & Kavelaars, J. J. 2006, *ApJ*, 636, 90
- Harris, W. M. 2003, in “Extra-Galactic Globular Cluster Systems” (ed. M. Kisspler-Patig) (Springer-Verlag, New York).
- Hills, J. G. 1980, *ApJ*, 235, 986
- Hunter, D. A., O’Connell, R. W. O., Gallagher, J. S., & Smecker- Hane, T. A. 2000, *AJ*, 120, 2383
- Hunter, D. A., Elmegreen, B. G., Dupuy, T. T., & Mortonson, M. 2003, *AJ*, 126, 1836
- Kharchenko, N. V., Piznukov, A. E., Roser, S., Schilbach, E., & Scholz, R.-D. 2005, *A&A*, 438, 1163
- Lada, C. J., Margulis, M., & Dearborn, D. 1984, *ApJ*, 285, 141L
- Lada, C. J., & Lada, E. A. 2003, *ARA&A*, 41, 57
- Lamers, H. J. G. L. M., Gieles, M., & Portegies Zwart, S. F. 2005, *A&A*, 429, 173 (LGPZ05)
- Larsen, S. S. 2002, *AJ*, 124, 1393
- Larsen, S. S. 2005, “Star Formation in Clusters”, in *Planets to Cosmology: Essential Science in Hubble’s Final Years*, ed., M. Livio (Cambridge: Cambridge University Press) (astro-ph/0408201)
- Larsen, S. S. 2006, “Observational Constraints on Cluster Evolution”, in *Mass Loss from Stars and the Evolution of Stellar Clusters*, ed., A de Koter, R. Waters & L. Smith, ASP Conference Series, Vol \*\*\* (San Francisco: ASP) (astro-ph/0609062)
- Larsen, S. S., & Richtler, R. 1999, *A & A*, 345, 59
- Li, Y., & Burstein, D. 2003, *ApJ*, 598, L103
- Maraston, C., Bastian, N., Saglia, R. P., Kissler-Patig, M., Schweizer. F., & Goudfrooij, P. 2004, *A&A*, 416, 467
- Mathis J. S. 1990, *ARA&A*, 28, 37
- Mengel, S., Lehnert, M. D., Thatte, N., & Genzel, R. 2005, *A & A*, 443, 41
- Oey, M. S., & Clarke, C. J. 1998, *AJ*, 115, 1543
- Puzia, T. H., Perrett, K. M., & Bridges, T. J. 2005, 434, 909
- Rafelski, M & Zaritsky, D. 2005, *AJ*, 129, 2701
- Rockosi, C. M. et al. 2002, *AJ*, 124, 349



- Ubeda, L., Maiz-Apelaniz, J., & Mackenty, J. 2006, AJ. in press
- Vesperini, E. 1998, MNRAS, 299, 1019
- Vesperini, E., & Zepf, S. E. 2003, ApJ, 587, L97
- Waters, C. Z., Zepf, S. E., Lauer, T. R., Baltz, E. A., & Silk, J. 2006, in press
- Weidner, C., Kroupa, P., & Larsen, S. S. 2004, MNRAS, 350, 1503
- Wielen, R. 1971, A&A, 13, 309
- Whitmore, B. C. 2003, The Formation of Star Clusters, in “A Decade of HST Science”, eds, Mario Livio, Keith Noll, & Massimo Stiavelli (Cambridge:Cambridge University Press), 153
- Whitmore, B. C. 2004, in ASP Conf. Ser. 322, “The Formation and Evolution of Massive Young Star Clusters”, ed. H. J. G. L. M. Lamers, L. J. Smith, & A. Nota (San Francisco: ASP), 411
- Whitmore, B. C., & Schweizer, F. 1995, AJ, 109, 960
- Whitmore, B. C., Zhang, Q., Leitherer, C., Fall, S. M., Schweizer, F., & Miller, B. W. 1999, AJ, 118, 1551
- Whitmore, B. C., & Zhang, Q. 2002, AJ, 124, 1418
- Zhang, Q., & Fall, S. M. 1999, ApJ, 527, L81
- Zhang, Q., Fall, S. M., & Whitmore, B. C. 2001, ApJ, 561, 727

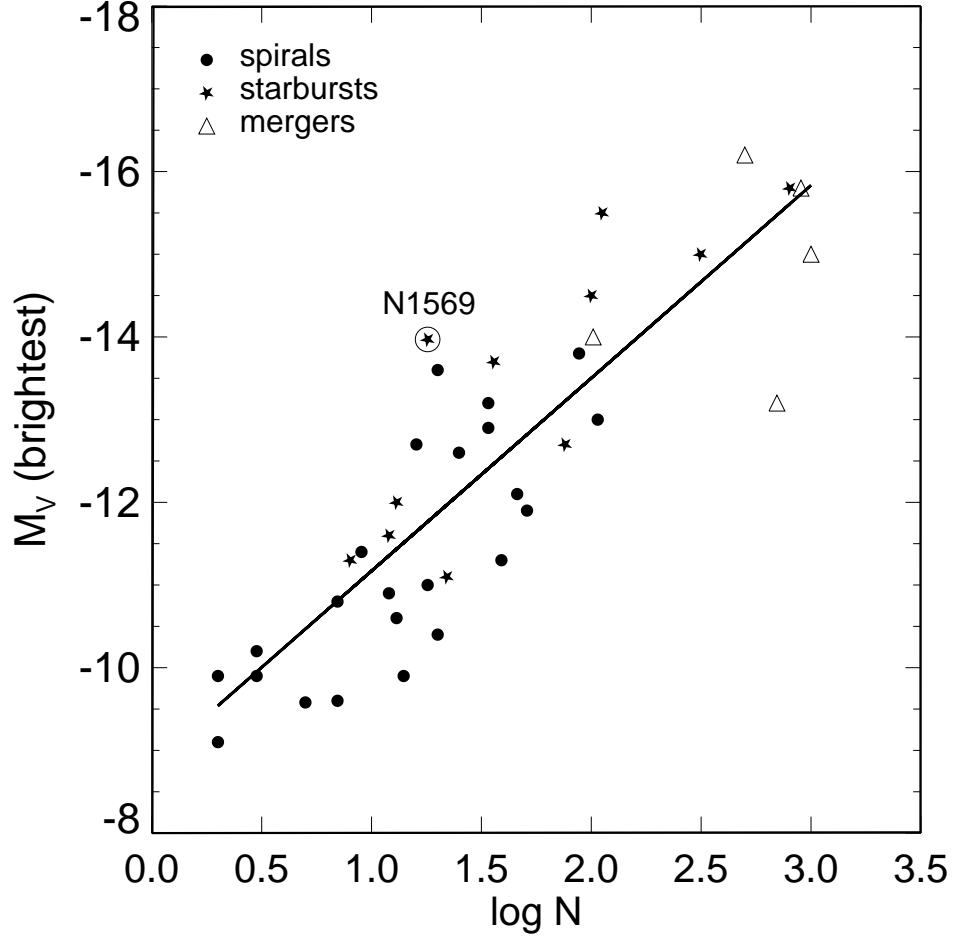


Fig. 1.— Magnitude of the brightest cluster against log of the number of clusters brighter than  $M_V = -9$  for 40 galaxies. The solid line shows the best fit, which has a slope  $-2.3 \pm 0.2$ .

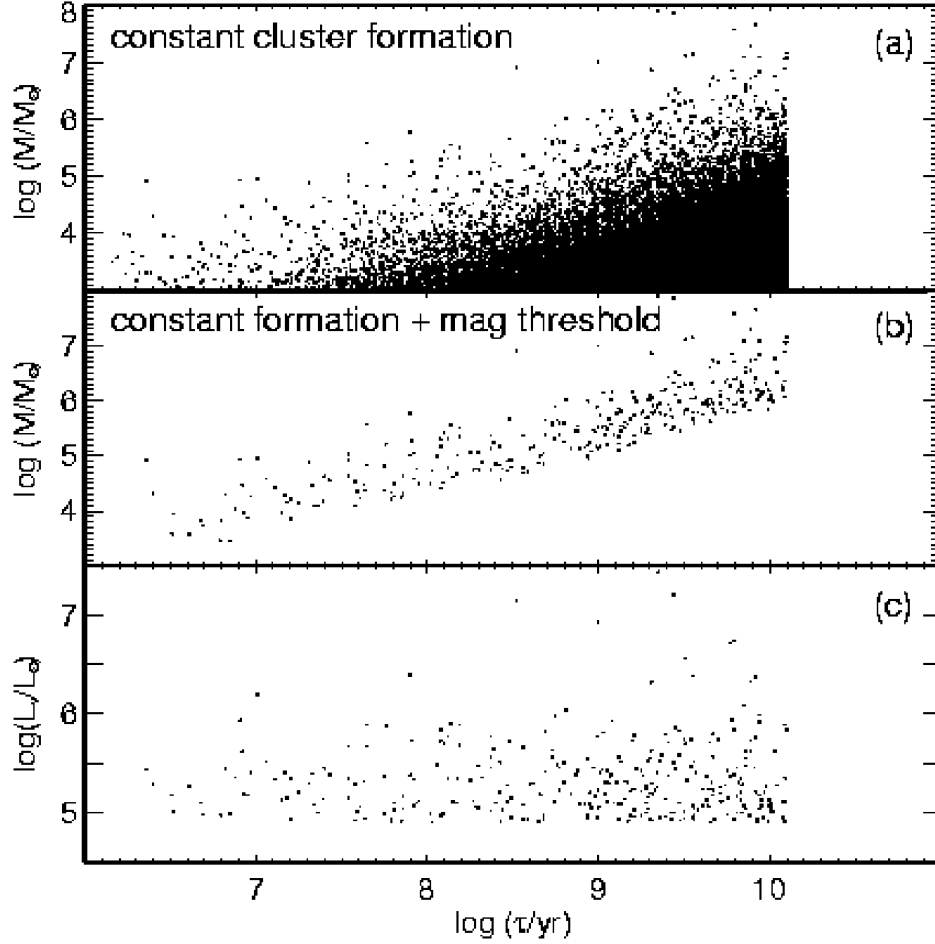


Fig. 2.— Synthetic cluster population formed at a constant rate for clusters with mass  $> 10^3 M_\odot$ . The top panel shows the age versus mass distribution, which has been drawn randomly from a power law mass function which has an index  $\beta = -2$ . The middle panel shows the age versus mass diagram for the same model, but with a V magnitude limit imposed to mimic observations. The bottom panel shows the V band luminosity versus the age distribution of the synthetic cluster population, including the magnitude limit.

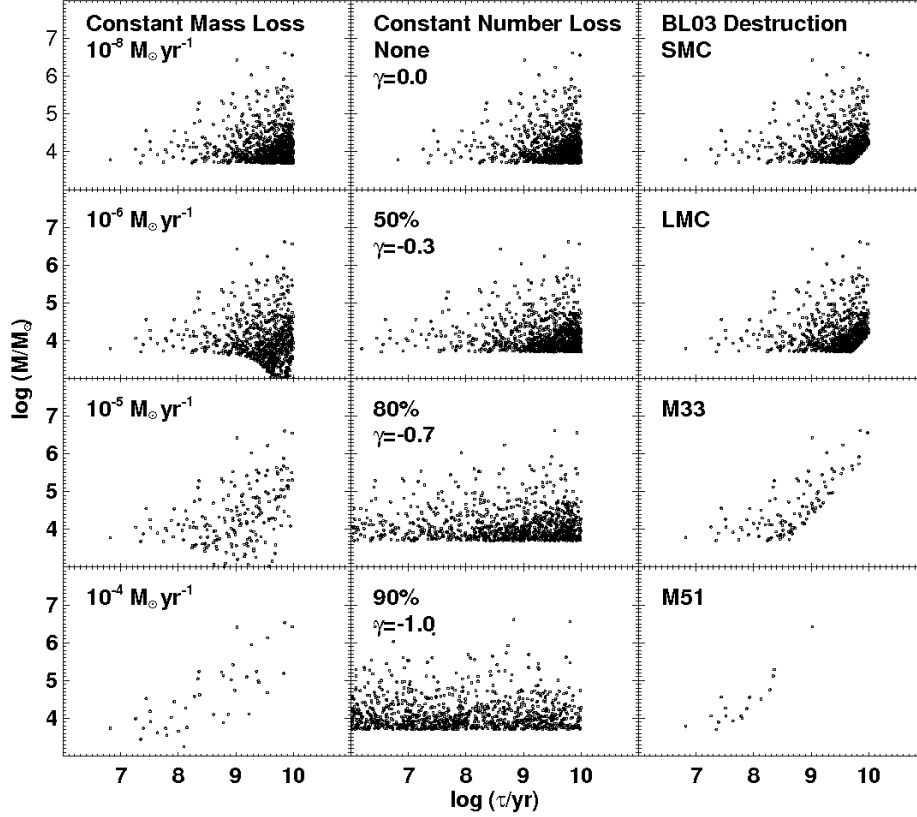


Fig. 3.— Age versus mass for a constant cluster formation model, which has been modified by twelve different disruption laws (described in the text). The left column of panels shows different values of constant mass loss (i.e., two-body relaxation; see Fall & Zhang 2001), the second column shows constant number loss (i.e., “infant mortality”), and the last column shows the resulting cluster population for the mass-dependent disruption model proposed by Boutloukos & Lamers (2003; BL03). The parameters for the BL03 disruption law are derived for the LMC by de Grijs & Anders (2005), and for the SMC, M33, and M51 by LGPZ05. Note that for illustrative purposes, we have plotted the infant mortality law (second column) beyond the first 100 Myr, although we do not believe it is physically relevant beyond this age (see text).

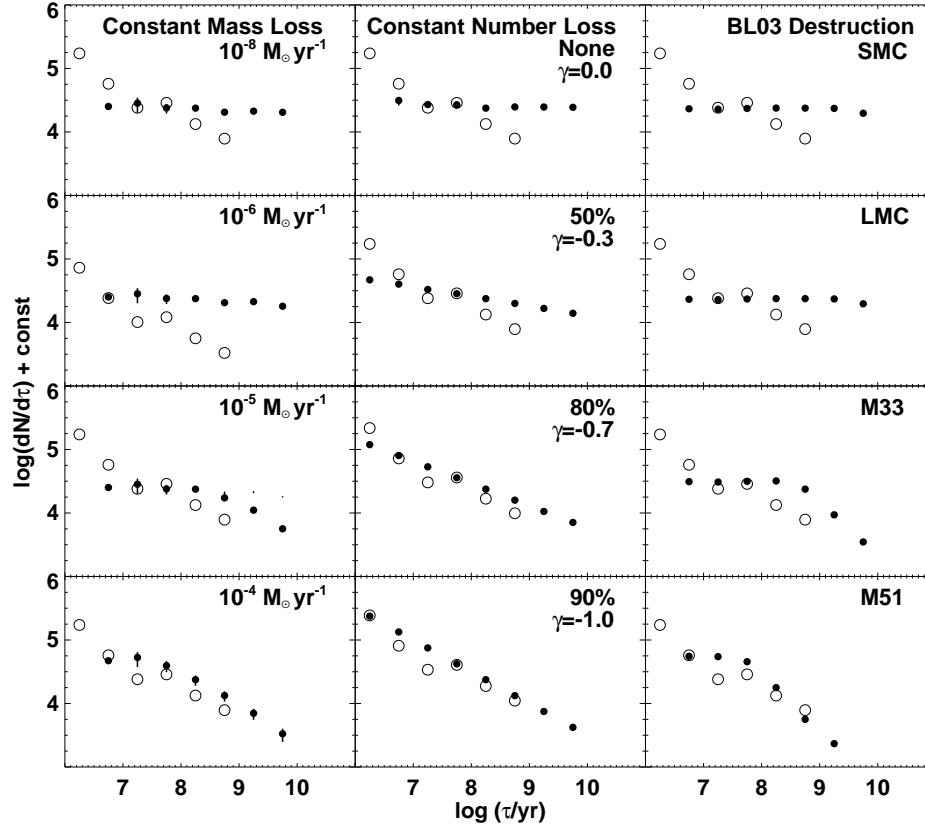


Fig. 4.— Age distribution (with arbitrary offset) for the twelve simulated models shown in Figure 3 (solid circles). For comparison, we show the completeness corrected age distribution for clusters in the Antennae galaxies with masses  $\geq 10^5 M_{\odot}$  (open circles).

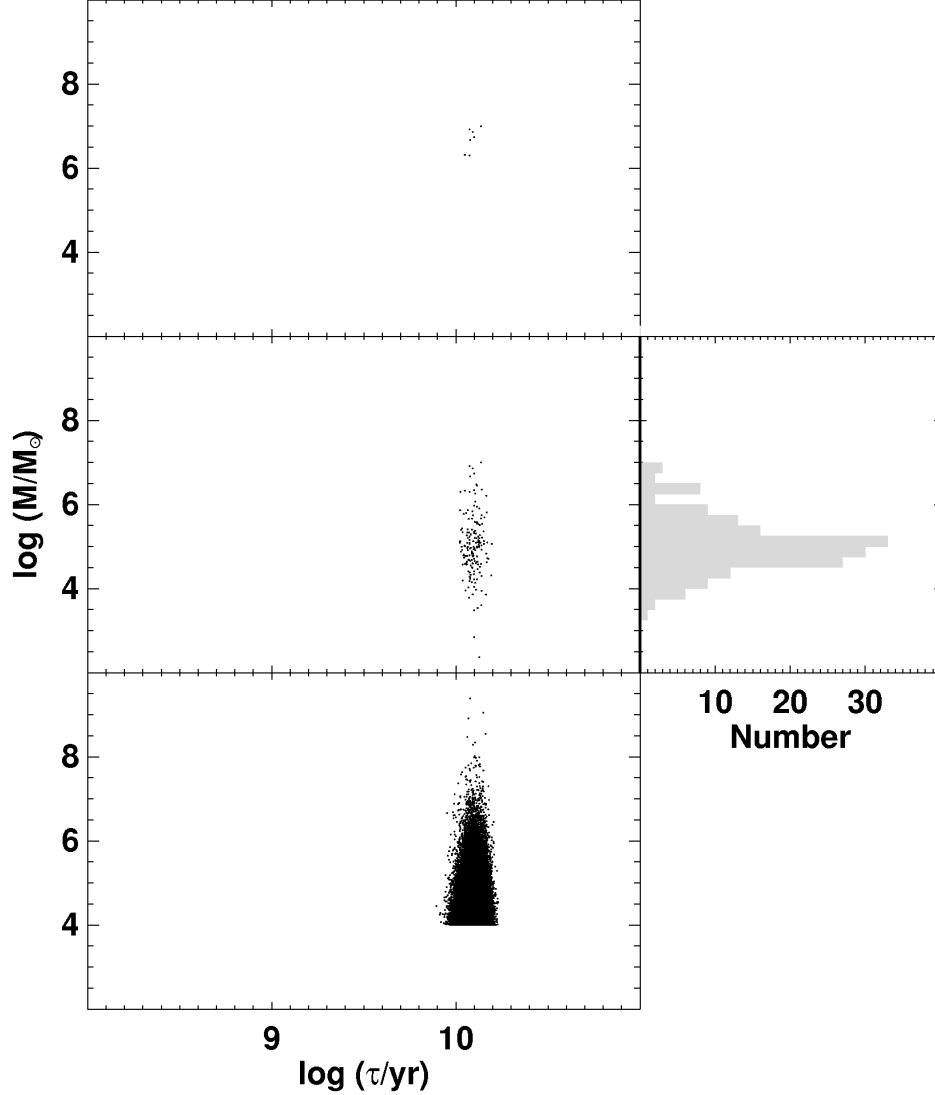


Fig. 5.— Simulation showing original (bottom panel,  $N=200,000$ ), surviving (middle panel,  $N=175$ ), and observable clusters (top panel,  $N=7$ ) for an ancient Gaussian burst model at the distance of the Antennae. These were formed assuming a power law mass function with  $\beta = -2$ , a Gaussian burst with a mean age of 12.6 Gyr, and a width of 1 Gyr. The initial cluster population was then subjected to our two-stage disruption model, as described in the text. The grey histogram shows that the resulting mass distribution after  $\sim 13$  Gyr has a peak mass  $\sim 10^5 M_\odot$ , similar to what is found for the Galactic globular cluster system.

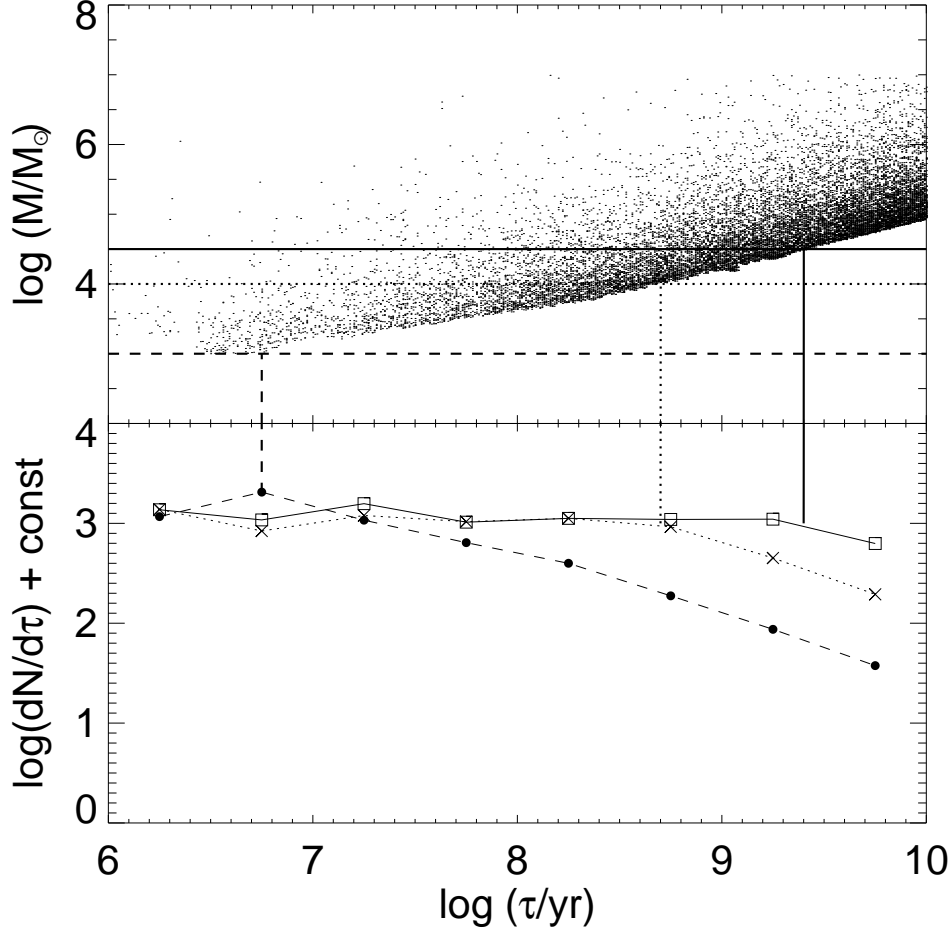


Fig. 6.— A constant cluster formation model with no disruption and an arbitrary V band detection limit that imposes a diagonal lower limit to the dataset (top panel). The horizontal lines represent different cluster mass cuts that might be used to study the sample. The bottom panel shows that as the mass limit used for plotting the age distribution is lowered from  $10^{4.5}M_\odot$  to  $10^3M_\odot$ , the age distribution goes from flat to having an apparent bend. The vertical lines show that the location of the bend correlates with the age at which incompleteness due to the magnitude limit occurs.

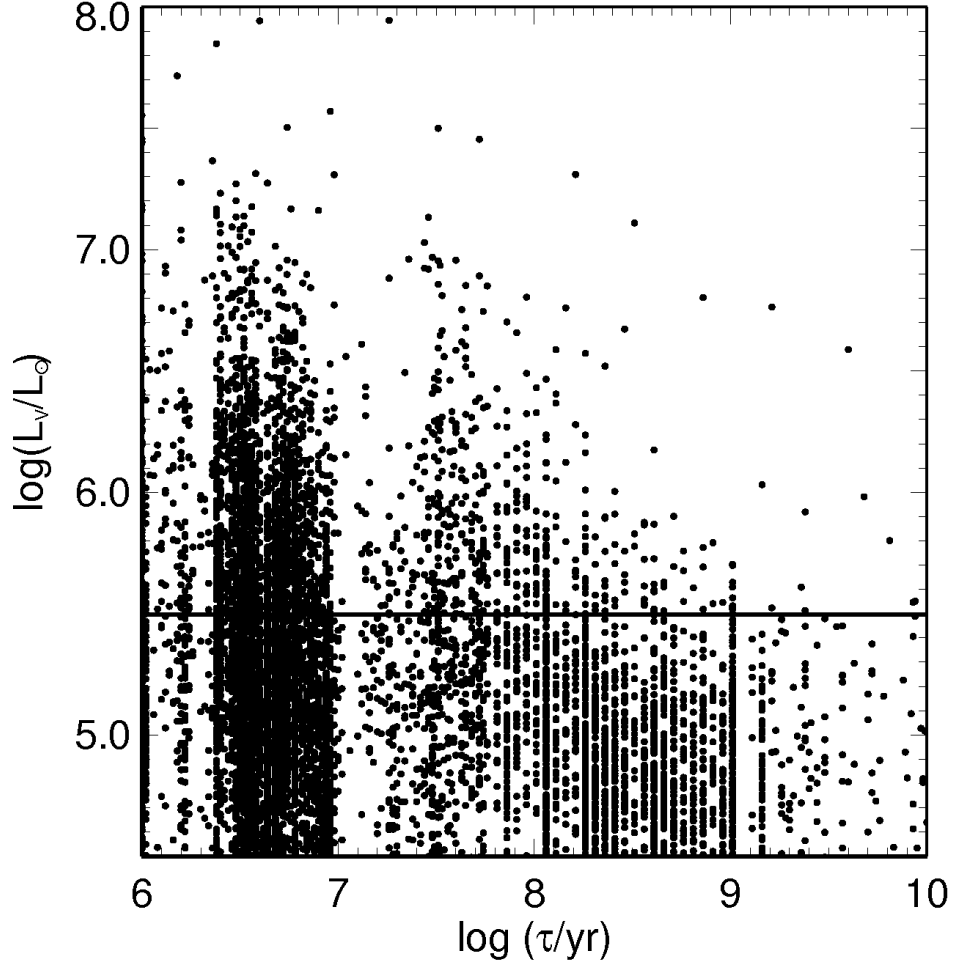


Fig. 7.— Log luminosity versus log age diagram of star clusters in the Antennae galaxies (as shown in Fall et al. 2005).  $L/L_\odot$  is the extinction corrected luminosity in the V-band. The horizontal line at  $L = 3 \times 10^5 L_\odot$  is the approximate upper limit for stellar contamination.



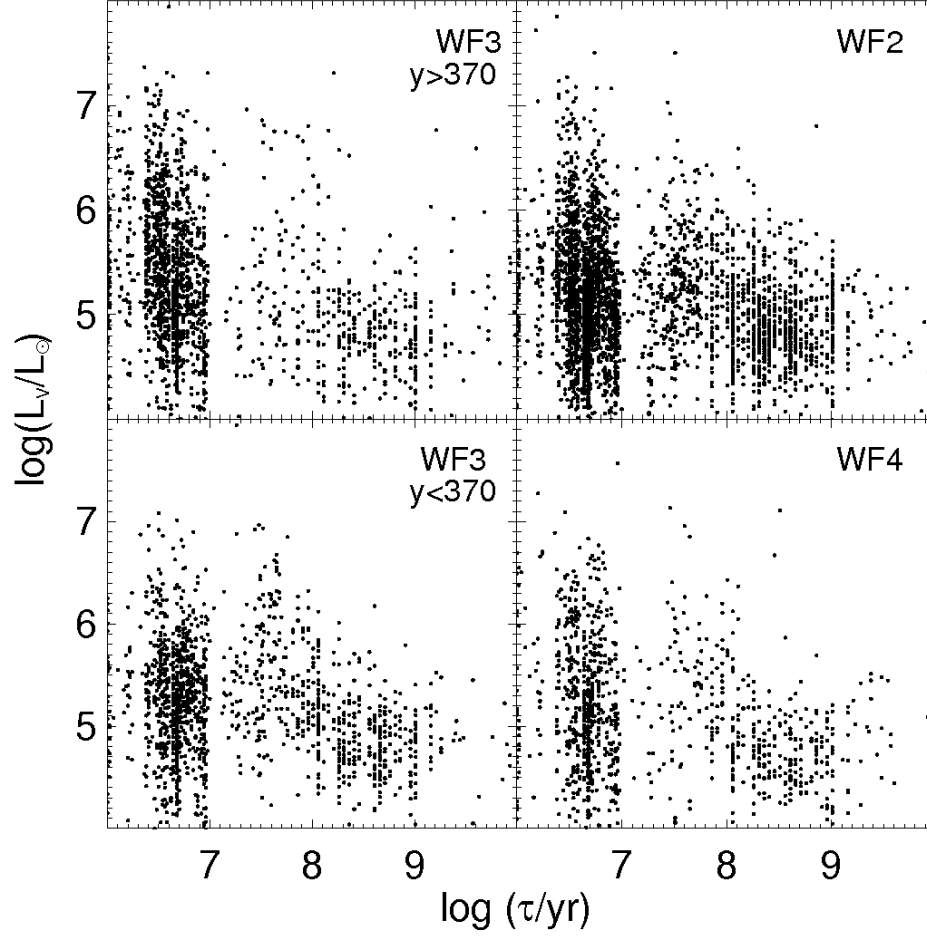


Fig. 8.— Log luminosity versus log age of Antennae clusters on different CCD chips. Note that the distribution on the WF3 chip is broken into two groups; the dusty “overlap region” ( $Y>370$ ), and the dust-free region ( $Y<370$ ) with fewer very young clusters

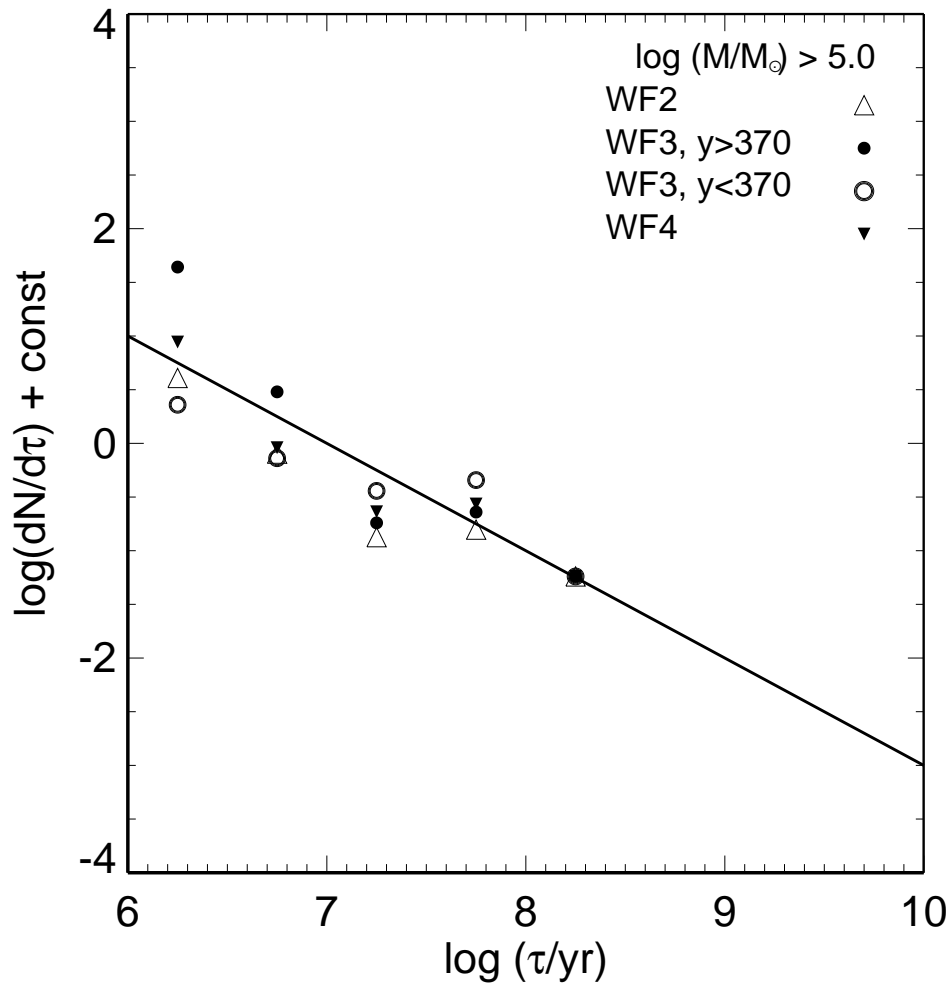


Fig. 9.— Age distribution for the Antennae cluster system for different CCD chips (normalized at  $\log \text{age} = 8.25$ ), as defined in Figure 8. The solid line is  $\gamma = -1$ .

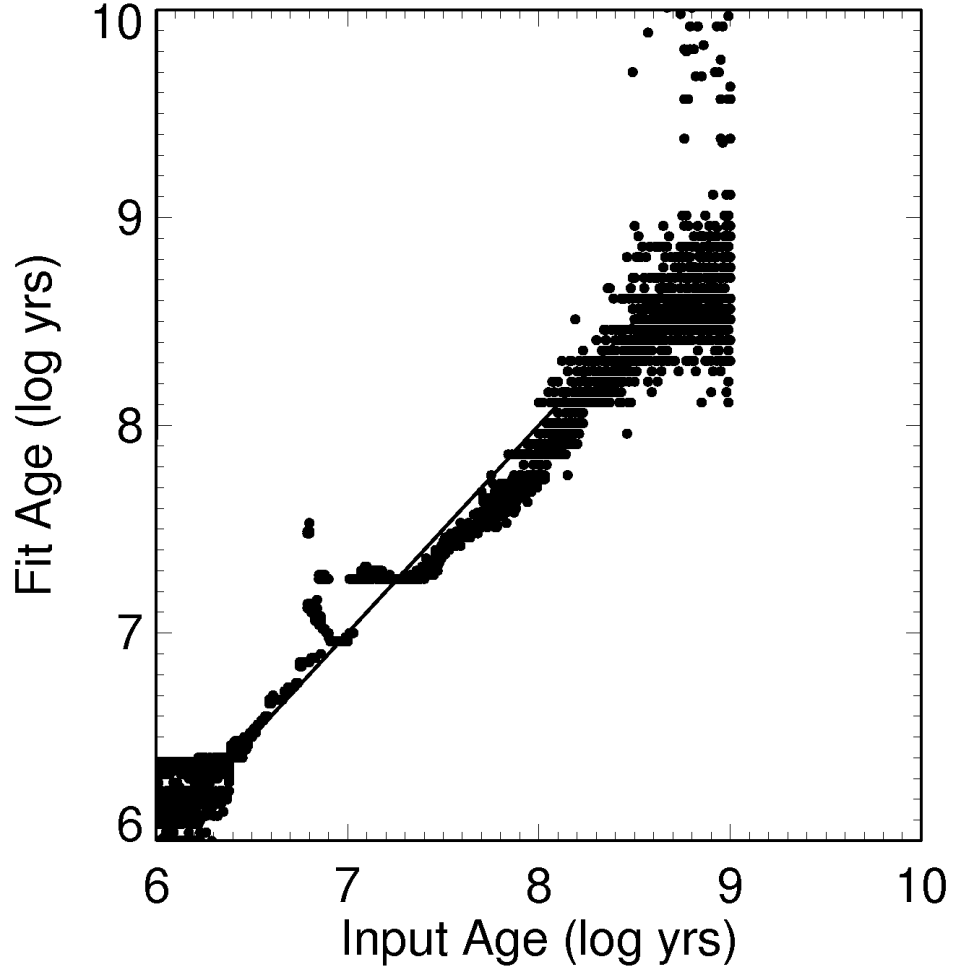


Fig. 10.— Results of age-dating a synthetic cluster population (input versus output age). The solid line shows one-to-one correspondence. The technique is described in the text.

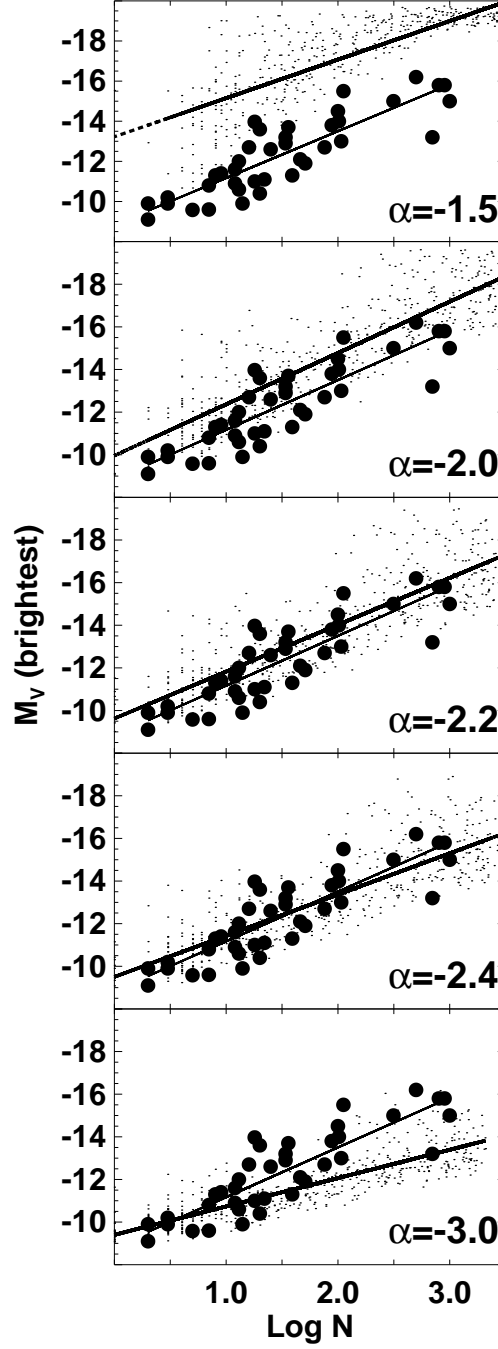


Fig. 11.— Maximum observed cluster magnitude versus log of the total number of clusters brighter than  $M_V = -9$  from our 500 Monte Carlo simulations (small dots). The simulations are compared with observations of cluster in 40 star-forming galaxies (filled circles), as described in the text. The results are shown for five different values of  $\alpha$ , the power law index for the cluster luminosity function.

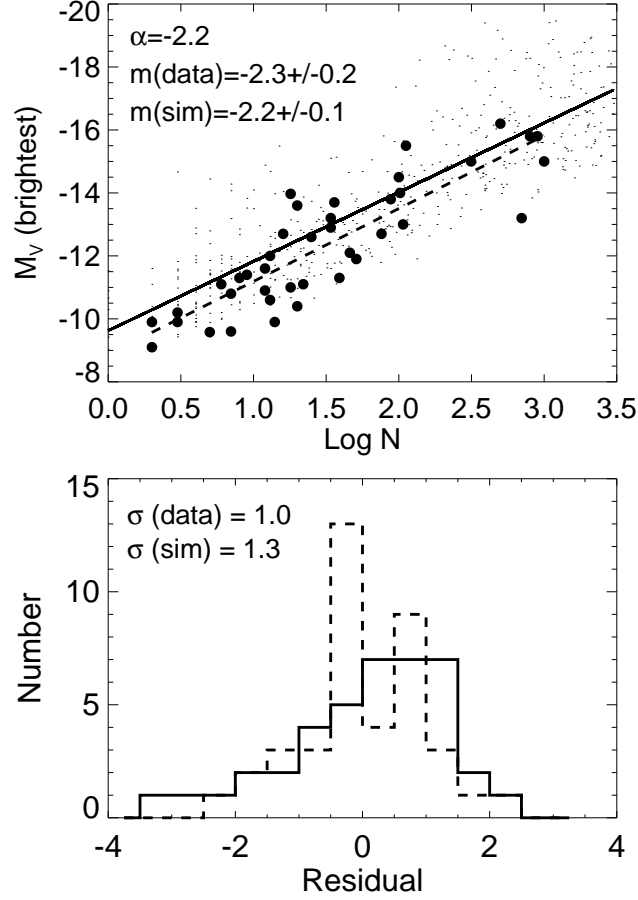


Fig. 12.— The top panel reproduces the comparison between our  $\alpha = -2.2$  simulation (solid line) and data (dashed line) for the  $M_V$  (brightest) versus  $\log N$  diagram, as shown in Figure 11. The best fit slopes are given for both. The bottom panel shows the dispersion ( $\sigma$ ) of the residuals in the data and simulations. These are tabulated for all studied values of  $\alpha$  in Table 1.

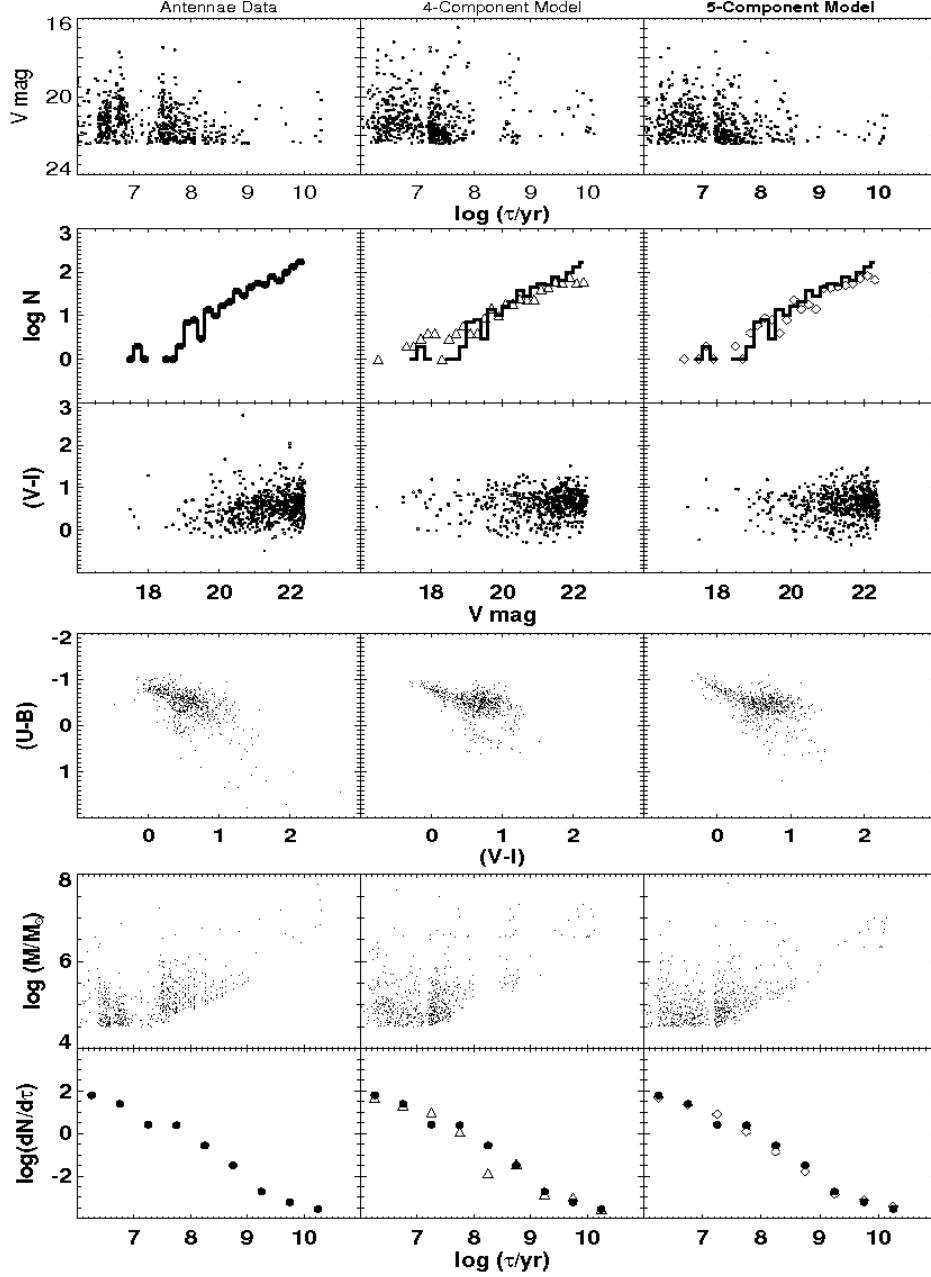


Fig. 13.— The first column shows several observed and derived diagnostics for the Antennae cluster system. The second column shows the same diagnostics for our original 4-component model for the Antennae, and the third column shows the diagnostics for our final 5-component model (as described in §3.2).

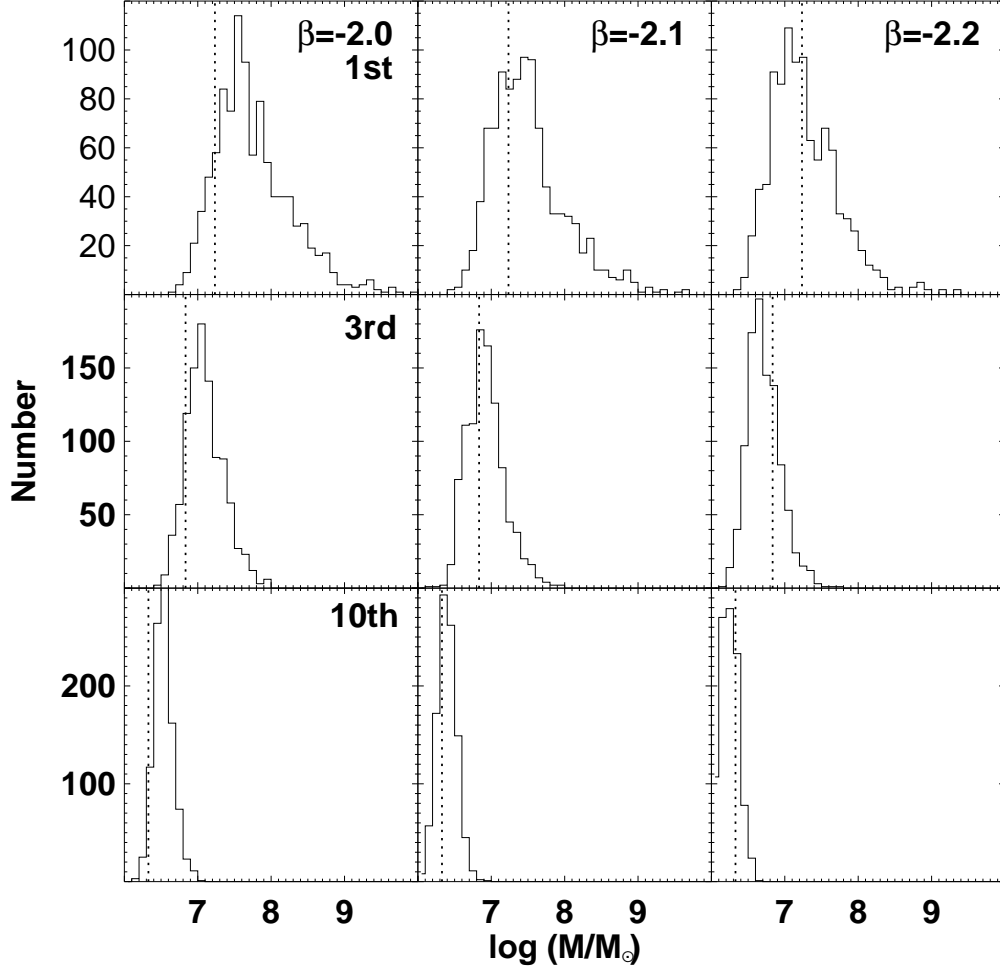


Fig. 14.— Mass distributions for the first, third, and tenth most massive cluster produced in 1000 Monte Carlo simulations. The total number of clusters used in each simulation is matched to the observed mass distribution in the range  $4.5 \geq \log M/M_\odot \geq 5.5$  for the young Antennae cluster population ( $10^6 \leq \log \tau \leq 10^8$ ). The three columns show simulations for  $\beta$  values of  $-2.0$ ,  $-2.1$ , and  $-2.2$ , and the dashed lines show the measured mass for the Antennae cluster system. The match between simulations and measurements show that a value of  $\beta = -2.1$  provides good fits without the need for a physical cutoff to the allowed cluster masses in the Antennae.

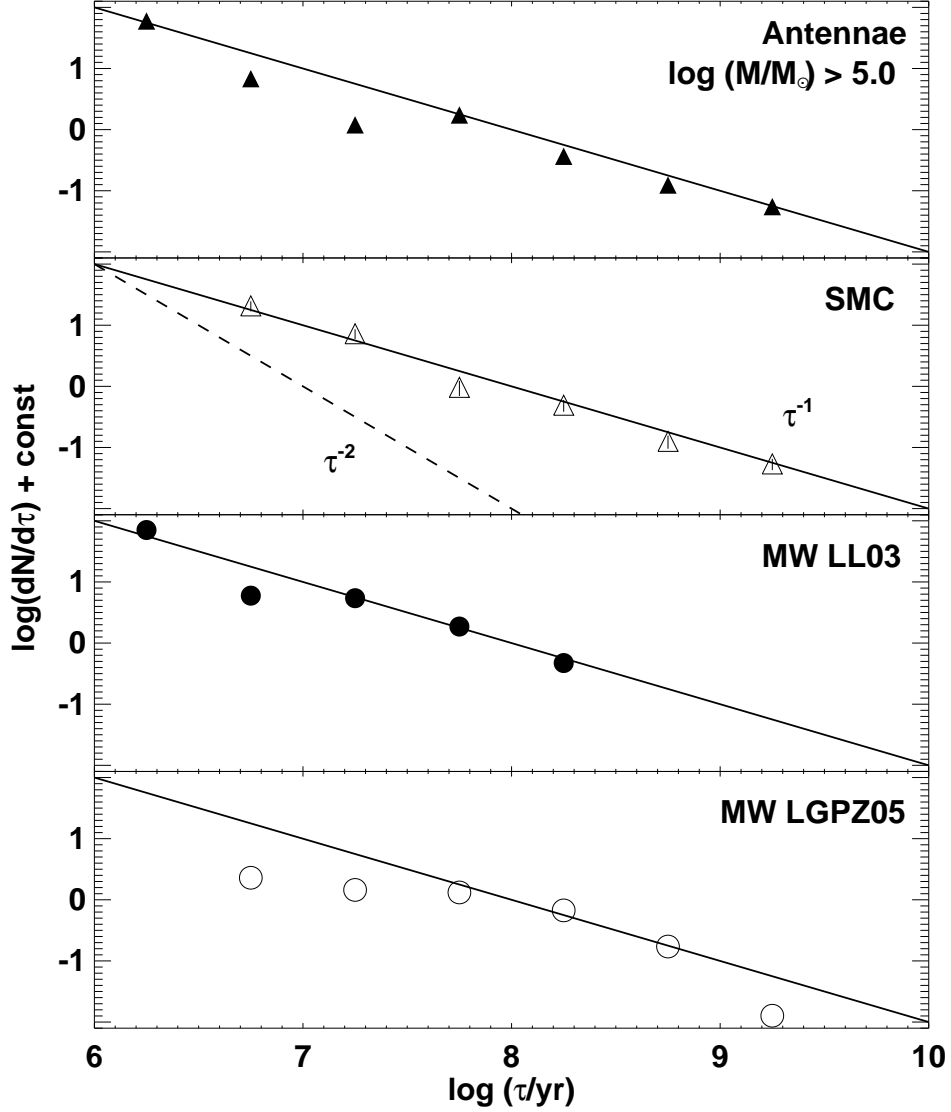


Fig. 15.— The age distribution for clusters in the Antennae with masses  $\geq 10^5 M_\odot$  (filled triangles); the SMC cluster population from Rafelski & Zaritsky (2005) but reinterpreted by Chandar, Fall, & Whitmore (2006); the embedded clusters in the Milky Way (filled circles; Lada & Lada 2003); and the open cluster sample of Kharchenko et al. (2005) as studied by LGPZ05 (open circles). The solid lines in each panel show  $dN/d\tau \propto \tau^\gamma$ , with  $\gamma = -1$ , and the dashed line in the second panel shows  $\gamma = -2$  from Rafelski & Zaritsky (2005) (see Chandar, Fall, & Whitmore, 2006, for a discussion).



Table 1. Results from  $M_V(\text{brightest})$  versus  $\log(N)$  Model Simulations

Powerlaw Index		Stdev of Residuals	
$\alpha$	Slope	$M_V(\log[N]=1.5)$	$\sigma$
–1.5	–1.9	–16.0	1.2
–2.0	–2.4	–13.6	1.3
–2.2	–2.2	–12.9	1.3
–2.4	–1.9	–12.4	1.2
–3.0	–1.3	–11.4	0.9
data <sup>a</sup>	–2.3	–12.4	1.0

<sup>a</sup>The data for 40 galaxies have been collected from the literature, as described in the text.

Table 2. Final Results of Toy Model for the Antennae

Galaxy property	Antennae		5-Component Model				
	galaxy	Total	#1 (const)	#2 (GC)	#3 (200 Myr)	#4 (1–100)	#5 (1–10)
stellar mass	5e10	3.8e10	1.2e10	1.2e10	6.4e9	4.6e9	2.5e9
total $M_V$	–21.7	–22.2	–18.7	–18.1	–20.1	–21.1	–21.6

References. — #1 = continuous creation over lifetime of the galaxy (1 Myr–13 Gyr)  
#2 = ancient Gaussian burst at  $12.6 \pm 1$  Gyr (i.e., old globular cluster population)  
#3 =  $200 \pm 100$  Myr Gaussian burst (i.e. initial encounter)  
#4 = 1 – 100 Myr continuous creation  
#5 = 1 – 10 Myr continuous creation (recent burst observed on CCD WF3)